Solar tracking evaluation and comparison towards a competitive Solar Challenger race vehicle

by

Jacobus Cornelius Faber

Dissertation submitted in fulfilment of the requirements for the degree

MASTER of ENGINEERING in ELECTRICAL ENGINEERING (M_ENGE)

in the

Department of Electrical, Electronic and Computer Engineering

in the

Faculty of Engineering, Built Environment, and Information Technology

at the

Central University of Technology, Free State

Supervisor:
Nicolaas Luwes, D.Tech.

BLOEMFONTEIN

2021

Declaration

I, Jacobus Cornelius Faber (Identity Number: _____; Student Number _____) do hereby declare that this research project which has been submitted to the Central University of Technology for the degree Master of Engineering: Electrical Engineering, is my own independent work, and complies with the Code of Academic Integrity, as well as other relevant policies, procedures, rules and regulations of the Central University of Technology, and has not been submitted before by any person in fulfilment (or partial fulfilment) of the requirements for the attainment of any qualification.

11/10/2021

Signature

Date

Acknowledgements

I would like to acknowledge the following individuals and institute, without whom the completion of this dissertation would not have been possible:

- my Creator, God Almighty, for granting me the perseverance to complete this project and dissertation;
- my family for all their support;
- my sister, Jani Faber, for all her support and encouragement;
- my study leader, Prof N. Luwes, for all his guidance and wisdom during the project, for his friendship as well as his endless patience;
- the Central University of Technology and RGEMS Research Unit for granting me the opportunity to undertake this project, for the monetary assistance, and the knowledge and experience gained during this project;
- the NRF for their monetary assistance; and
- all my friends at RGEMS for their help in the setup of the project, as well as for their moral support.

Abstract

Observed global economic growth increases the demand for energy that is currently, especially in South Africa, generated with unsustainable fossil fuels. A substantial energy user is mobility that includes transportation. It seems that future markets are searching for alternative greener energy sources. One of the largest accessible sources of sustainable energy on earth is the sun, with a large drive of sustainable energy supply aiming at solar power. A sustainable mobility option would be solar powered vehicles and the Sasol Solar Challenge is a testing and development platform for this new technology. The South African Sasol Solar Challenge is a biannual competition and claims to be the ultimate test of technology and innovation. Being the ultimate technology test, it sees the development of some of the world's most innovative energy technologies. Solar challenger vehicles are prototypical, fully electric vehicles, developed by research and competitive teams. The technology developed by these teams, similar to Formula 1 (F1) racing, might be seen in some form or another in electric vehicles of tomorrow. Events like the Sasol Solar Challenge accelerate research into more efficient solar cells, solar panels (also known as solar modules or PV modules), batteries, semi-autonomous vehicle technology, and battery management and protection systems.

This study evaluates and compares solar tracking options towards a competitive solar challenger vehicle. It evaluates a proposal of a transparent aerodynamic cover under which tracking solar panels (also known as PV modules) could move freely, without influencing the aerodynamic characteristic and drag coefficient of the vehicle. This includes test methods, test instrumentation and final evaluation for an optimal cover material. Results indicate the gains with solar tracking and losses of irradiation of cover material with tracking that needs to be considered for drag coefficient gains towards a competitive solar challenger race vehicle.

The study started by evaluating special cover materials, i.e. considering their chemical and physical properties. Then demonstrating the design, construction and testing of a scale-model instrument with which to evaluate and compare solar tracking, with and without such covering material. Thereafter it demonstrates the evaluation and comparison of solar tracking of the full-scale 2018 solar power challenger vehicle.

The results of small-scale experimentation led to alterations on the full-size solar vehicle design, which included bypass diode placements. The preselection of materials, the design of scale testing instrumentation and scale results compared to the full-scale results are discussed to indicate the gains and losses that occur for a proposed cover.

The scale model saw a 7% – 11% energy loss with the presence of the cover. On the full-size model this increased drastically to 20% – 33%. This large difference could be a result of the intense heat generated in the full-size model, as well as the environmental damage (scratches, sunburn) on the clear polycarbonate cover at the time of testing. Measurements were taken in all four cardinal directions.

Finding of the research study has showed an increase in power with tracking, but that the energy loss of the cover does not justify decreasing of drag coefficient, when traveling at low speeds. Using real-world measured power, one should, however, reconsider this loss in the drag coefficients of new designs and/or the physical protection of cover material or other factors, like aerodynamic stability and drag at higher speeds.

Table of Contents

List of Figures

List of Tables

List of Abbreviations

F1	Formula 1
PV	Photovoltaic
CAD	Computer Aided Design
Si	Silicon
PC	Polycarbonate
PMMA	Poly methyl methacrylate
PET	Polyethylene Terephthalate
SAN	Styrene Acrylonitrile
GPPS	General Purpose Polystyrene
PD	Photodiode
DC	Direct Current
BJT	Bipolar junction transistor
MOSFET	Metal Oxide Field-Effect Transistor
IGBT	Insulated Gate Bipolar Transistor
MPPT	Maximum Power Point Tracker
MPP	Maximum Power Point
STC	Standard Test Condition
Imp	Maximum Power Point Current
Vmp	Maximum Power Point Voltage
Voc	Open Circuit Voltage
Isc	Short Circuit Current
IV	Current Voltage
CV	Constant Voltage
SC	Short-Current Pulse
OV	Open Voltage

P&O	Perturb & Observe
IC	Incremental Conductance

Chapter 1: Introduction

1.1 Statement of the problem

The Sasol Solar Challenge is an international competition where national and international teams design and develop solar-powered vehicles to drive across South Africa. The teams are expected to travel on public roads in a vehicle that is roadworthy. The vehicles cover distances of 2 500 – 5000 km, with an altitude difference of about 2 000 m in 8 days [1]. Efficiency that leads to distance travelled in these competitive solar vehicles is of paramount importance. These challenger prototype designs are novel and innovative, showing custom designs in the pillars of technologies in power, weight and aerodynamics. The challenger class of vehicles must have a maximum solar array size of $4m^2$, that charge a battery with a certain size, and must be within specific dimensions.

Solar-powered challenger vehicles' main and only external power source is solar irradiation; solar tracking evaluation and comparison therefore needs to be done towards a competitive solar challenger race vehicle. Solar tracking is the act of tilting the photovoltaic (PV) module in the direction of the sun. This can be done on one axis or on a dual axis. One needs to consider that solar tracking could generate more power in vehicles, but at a cost of weight and aerodynamics. Solar tracking under an aerodynamic transparent cover would not increase aerodynamic drag and needs to be evaluated. The transparent cover could, however, introduce irradiation losses that translate to power losses, and needs to be evaluated against gains in other areas. In order to fully evaluate tracking with and without a cover the user needs to consider the different types of cover materials to use and how to evaluate these materials [2]. The computer-aided design (CAD) drawing in Figure 1 below shows the aerodynamic transparent dome solar tracking application developed and needs to be evaluated.

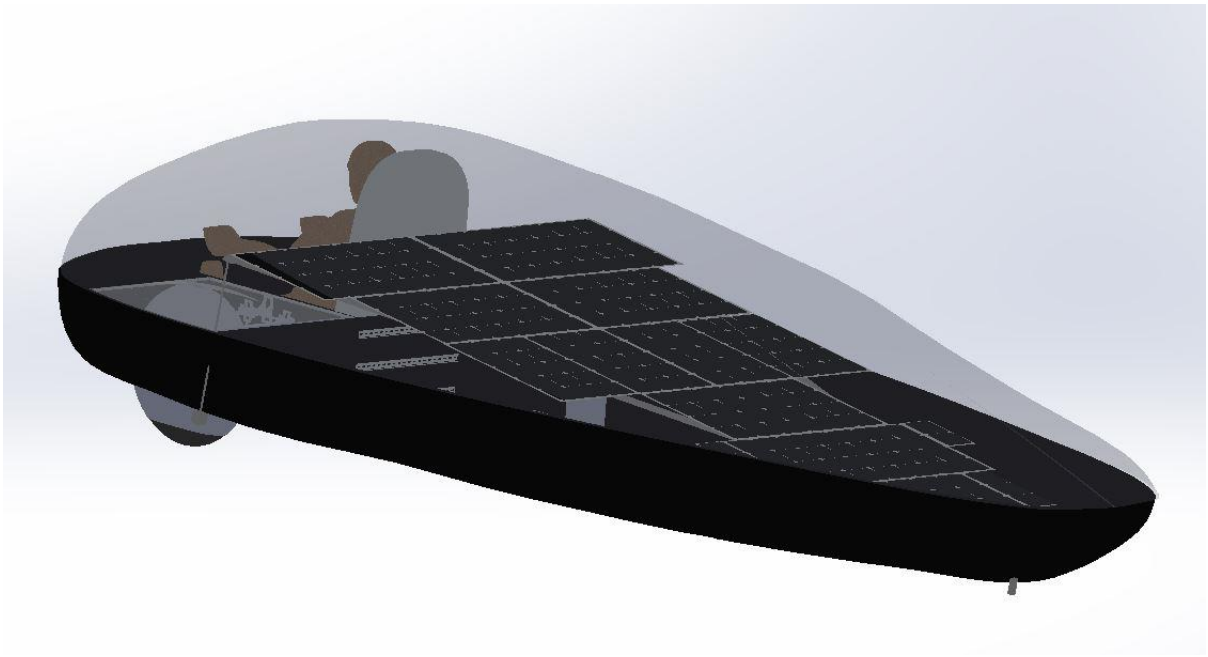

Figure 1 : CAD of Solar Challenge vehicle

The problem that needs to be solved, is how to generate solar tracking design inputs and considerations towards a competitive solar challenger vehicle. Solar tracking evaluation methods with their corresponding result interpretations need to be developed, evaluated, and discussed; this would include comparison with and without the suggested transparent cover that needs testing. This involves, inter alia, the identification of the optimal transparent cover material, evaluation of the solar tracking underneath such an aerodynamically shaped dome. Design inputs towards a competitive solar challenger vehicle with solar tracking, would include conclusions drawn towards whether aerodynamic gains outshine solar tracking gains, with the addition of an aerodynamically shaped dome made of optimal transparent material.

1.2 Aim of the investigation

Solar Challenge vehicles are designed with a unique combination of equipment and regulated by the Challenge rules and regulations. In short, Solar Challenge vehicles are driven by electric motors, powered by a set-size battery that is charged from a set-size solar module. At the Solar Challenge the

team that covers the longest distance in eight days, considering Challenge rules, is crowned victorious. The battery pack for this vehicle is built up of 18650 Li-ion batteries with the active components totalling up to 20 kg; this weight does not include the enclosure to secure the cells. These batteries are charged with 4 m² of Si PV modules, coated with a non-reflective surface. The battery pack is governed by an Orion battery management system that controls the charging, cell balancing, and temperatures. The motors are high-efficiency Marand in-hub motors, and the motor controller is the Tritium Wavesculptor 22, a lightweight controller. Photovoltaic (PV) modules are placed under a clear transparent cover (depicted in Figure 1) which will need ribs to keep the polymer cover from collapsing.

This study aims to compare and evaluate power gains and losses of solar tracking that include solar tracking with and without the proposed aerodynamic transparent cover. Results and discussions will give considerations towards a competitive solar challenger vehicle.

1.3 Hypothesis

The dissertation demonstrates the development of testing methods, test instruments and comparison of materials to compare and evaluate power gains and losses of solar tracking that include solar tracking with and without the proposed aerodynamic transparent cover. The corresponding resulted interpretations would give input on solar tracking towards a competitive solar challenge vehicle. These developed methods, with the corresponding resulted interpretations, include the evaluation of solar tracking under a transparent aerodynamically shaped dome that is related to a competitive Solar Challenge vehicle. This would entail that the hypotheses also include optimal material identification in order to compare solar tracking within a cover application towards a competitive Solar Challenge vehicle.

1.3 Research Question

- Develop tools and testing methods to gather and evaluate data that will be generated during this project.
- Study the impact on power gains and losses with an aerodynamic cover, compared to that of no cover.

1.4 Contributions

- Test instrument that was designed and build
- The data generated by the experiment

1.5 Layout of dissertation

- Chapter 1 defines the problem and aims and hypothesis.
- Chapter 2 is a literature study that explains the different types of components, giving a detailed explanation of all the different options considered.
- Chapter3 explains how the devices were evaluated and then tested. It also explains the methodology of how the project was calibrated and tested.
- Chapter 4 shows the results of the different tests and then the discussion thereof.
- Chapter 5 comprises the Conclusion.

Chapter 2: Review of the relevant literature

In order to evaluate and compare solar tracking towards a competitive solar challenger race vehicle, one must consider solar tracking as well as solar tracking under an aerodynamic dome. Power gains must be compared with aerodynamic gains, considering possible power generation losses through the dome material. This consideration incudes the determination of a suitable cover material to evaluate solar tacking under it. Evaluation and comparison of such a solar tracking setup necessitate the design and construction of evaluation methods and instrumentation, that evaluate solar tracking with and without such a cover or dome. In this section the Sasol Solar Challenge is discussed, thus indicating the need for an efficient power generation method, followed by PV panels, cover materials for a dome, light transmission and the selection of hardware needed for measuring and construction of instrumentation.

2.1 Sasol Solar challenge

The Sasol Solar Challenge is an event that sees different teams from across the world designing and building solar vehicles to travel across South Africa. The eight days of participation would test the vehicles' driving ability at different altitudes and in different biospheres. Three classes of solar power vehicles take part in the Sasol Solar Challenge, viz. the adventure class, cruiser class and the challenger class. Each of these classes has its own set of rules and regulations [1]. The challenger-class solar vehicle is designed for maximum energy efficiency and endurance. This vehicle is limited to 4 m^2 of silicon solar panels, and a 20-kg Li-ion battery. The challenger vehicle must also have four wheels. As this vehicle must travel along the South African highways, it must be robust enough to withstand the harsh road and atmospheric conditions. The driver must sit comfortably and have an easy means of egress within a specific time limit. All these requirements are to be met within the limited space and the design of the PV panels of the vehicle.

2.2 Photovoltaic (PV) Module

PV modules are devices that can generate electricity through the flow of electrons, using the irradiation from the sun. The material of the PV cell determines the band gap of the PV system. This band gap is the difference between the top of the valence band and the bottom of the conduction band in semiconductors. When electrons absorb light, they jump from the valance band to the conduction band and, in doing so, they produce electricity. This production of energy can be calculated below [3].

$$E = h * C/\lambda \qquad \textit{Equation 1}$$

Where:
E = Energy (J)
h = Planks Constant = 6.626x10^-34 (J*sec)
C = Velocity of light = 2.99x10^8 (m/sec)
λ = Wavelength (m)

Silicon (Si), for example, has a band gap of 1.2 eV; by using the above equation, the wavelength is calculated to be 1 030 nm [4]. Si PV modules are most efficient on light wavelengths from 500 nm – 1 030 nm [5]. There are different kinds of industrial PV modules, but only a few that fit the criteria of solar vehicle regulations, including the fact that PV modules must be lightweight, flexible, and durable.

2.3 Covering Material

As proposed an aerodynamic solution for tracking PV modules or panels is a transparent dome. This entails a covering material to be used with solar tracking. The literature review shows that, despite the fact that there is an extensive list of covering materials, there are five prominent types that stand out and are compared. The difference in malleability among the five non-crystalline glassy polymers is related to their structures. The different polymers will be tabulated in order to be compared.

2.3.1 Polycarbonate

Polycarbonate is a transparent synthetic resin and considered a special type of polyester [6]. Polycarbonate has a vast array of applications across multiple fields. It is used in various industries – from the electronic to the medical field. The major advantage of polycarbonate over other plastics is its strength combined with light weight. It is about one-third of the weight of acrylic. It is commonly used in cell phone casings, bulletproof glass, eyewear lenses, automobile headlights, et cetera [7]. Polycarbonates (PC) have a similar chemical structure to polyester with only a few slight differences. Polyester contains an alcohol group (OR) connecting the terephthalate monomers, whereas PC contains a carbonyl group (CO) connecting the bisphenol monomers. This structural difference exhibited by PC, leads to its high-impact strength [8].

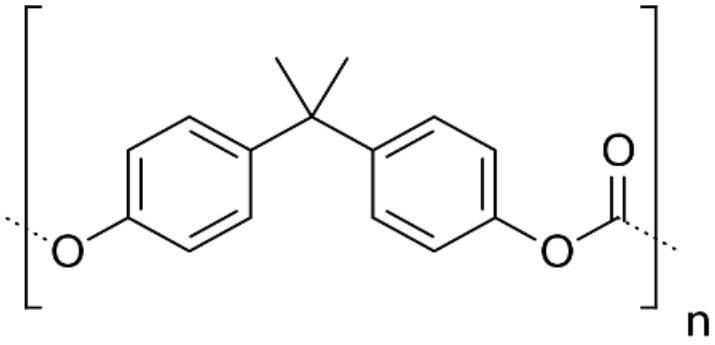

Figure 2 : Chemical structure of PC

The 2-by-2 propylidene group linking the two aromatic rings in PC, as seen above in Figure 2, allows for rotation in its structure, which is responsible for the flexibility of this polymer [6].

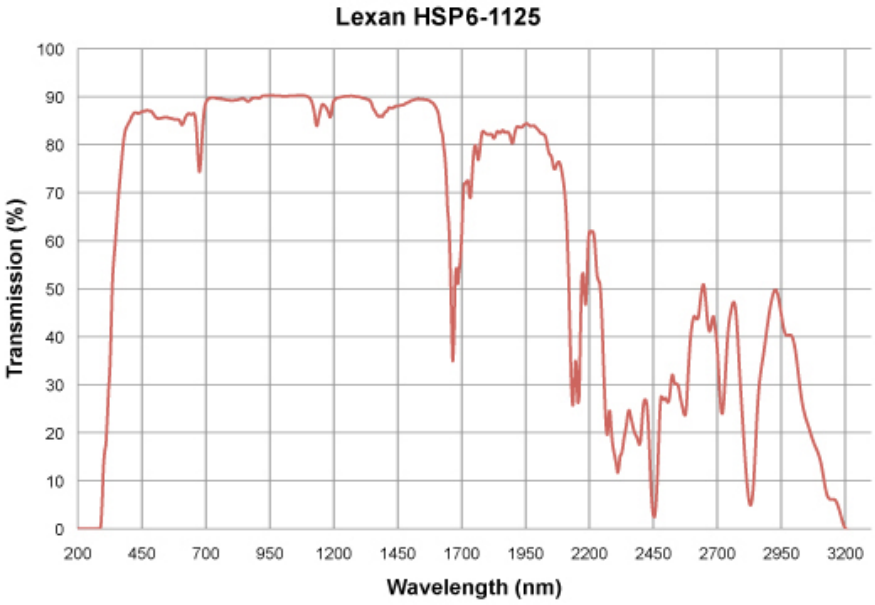

Figure 3 : Transmission curve of PC[10]

Figure 3 above depicts the transmission curve of a piece of Lexan PC. This curve shows the amount of light passing through different wavelengths. As can be seen, the visible spectrum falls in a high-transmission spectrum.

2.3.2 PMMA

Poly(methyl methacrylate) (PMMA) (see Figure 4) is a thermoplastic that is rigid at room temperature but becomes softer and malleable at higher temperatures [8]. The structural rigidity of PMMA leads to low impact strength [11]. PMMA is part of the acrylic family of polymers [11], and is commonly used in domed skylights, aircraft canopies, luminous ceilings, optical fibres, etc.

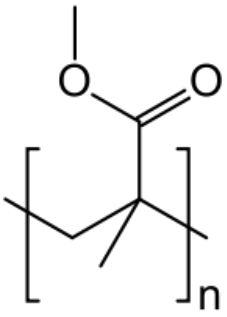

Figure 4 : Chemical structure of PMMA

The polymer, forming a rigid amorphous structure as it cools down, is held in place by strong dipole-dipole bonds from the carbonyl rather than cross-linking, which forms crystalline structures as

seen above in Figure 4 [13]. PMMA displays an intermediate level order in the polymeric stacking leading to its high clarity [14].

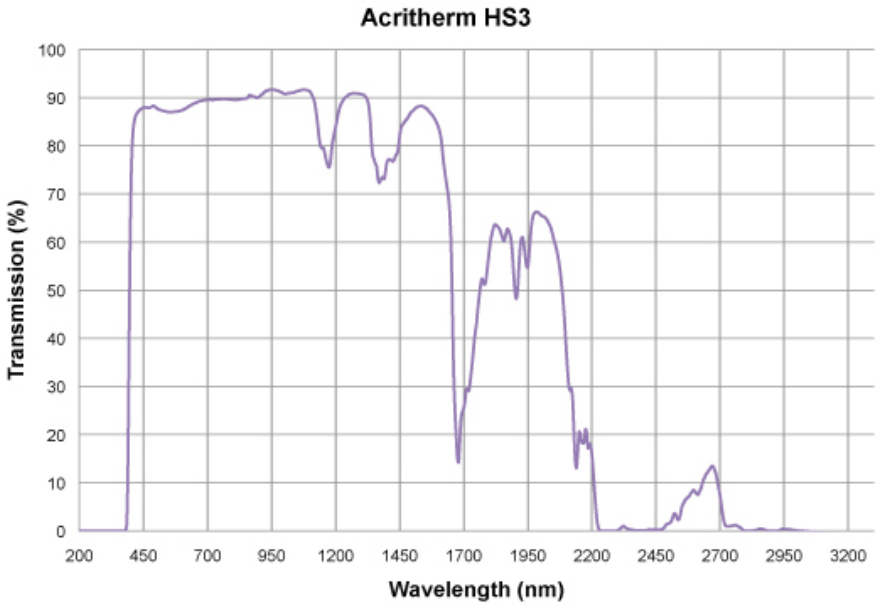

Figure 5 : Transmission curve of PMMA[10].

Figure 5 depicts the transmission curve of Acritherm PMMA.

2.3.3 PET

Polyethylene Terephthalate (PET) forms part of the general purpose of polymers. It is part of the polyester family, and known for its strength and stiffness [15]. It is known for its excellent combination of, inter alia, mechanical, thermal, and chemical properties. This is also a heavy polymer sitting at 1.34g/cm³ [16].

PET boasts a wide range of uses: from the most common use in recyclable soft-drink bottles, to thin-film solar cells [17].

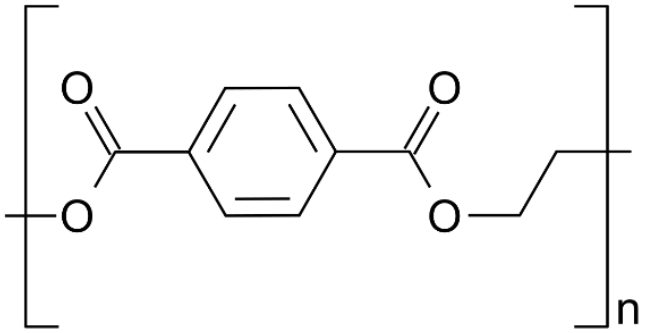

Figure 6 : Chemical structure of PET

Figure 6 above depicts the chemical structure of PET. It forms a flexible plastic that is easily scratched. The large aromatic rings present in PET provide the polymer with its stiffness and strength [15].

2.3.4 SAN

Styrene Acrylonitrile (SAN) is a copolymer resin consisting of styrene and acrylonitrile [18]. The addition of butadiene to SAN forms acrylonitrile butadiene styrene (ABS), with a visibility range of greater than 90% [19]. SAN has great toughness and chemical resistance, but experiences difficulty in moulding and transparency [20]. It is commonly used in automobile parts, appliances, kitchenware, etc.

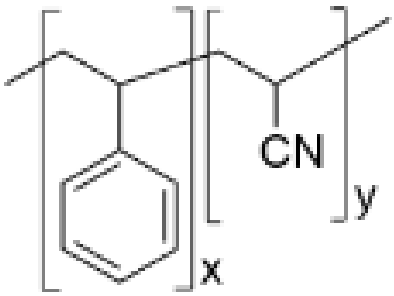

Figure 7 : Chemical structure of SAN

Figure 7 depicts the structure of Styrene Acrylonitrile copolymer (SAN) consisting of two monomers, styrene (x) and acrylonitrile (y) in a 70:30 ratio [18][19].

2.3.5 General-purpose Polystyrene (GPPS)

General-purpose Polystyrene (GPPS) is a hard, stiff, and transparent synthetic polymer with a low mass-to-volume ratio [21]. It is the simplest plastic consisting of styrene [22]. GPPS has a high reflective index [19][23][24]. It is commonly used in the food industry in its rigid (trays and containers) and foamed (cups and plates) forms [21].

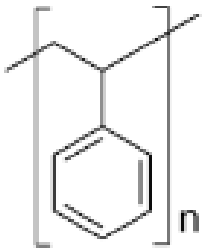

Figure 8 : Chemical structure of GPPS

Figure 8 depicts the chemical structure of general-purpose polystyrene (GPPS). The transparency of this polymer is owed to the aromatic rings preventing close stacking. The prevention of rotation in the carbon-carbon bonds, due to the proximity of the aromatic rings to each other, results in the rigidity of the GPPS [21].

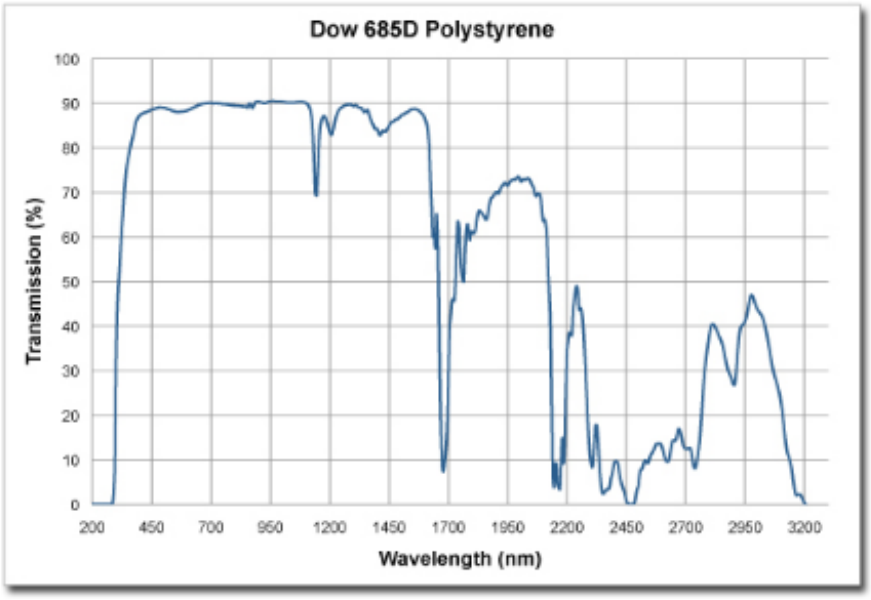

Figure 9 : Transmission curve of GPPS[10]

2.4 Light Transmission Obstacles

Having a cover over the panels introduces its own variables with light that must travel through it. The light passing through an object can be reflected, absorbed, or partially reflected and absorbed simultaneously. Solar generation is achieved by light being absorbed in the panel. The more the light is reflected, the less there is to be absorbed, whereas refracted light changes direction resulting in the angle of incidence being not optimal. The relevant theories below are considered.

2.4.1 Reflection

Reflection is the amount of light reflected away from an object. The angle of the ray of incidence is symmetric to the reflection ray [13]. According to the datasheet of PC and PMMA, they both have a reflection percentage of 4% [25].

2.4.2 Refraction

Refraction is an occurrence of light bending away from the normal when going through a clear polymer. This happens at different coefficients, depending on the polymer.

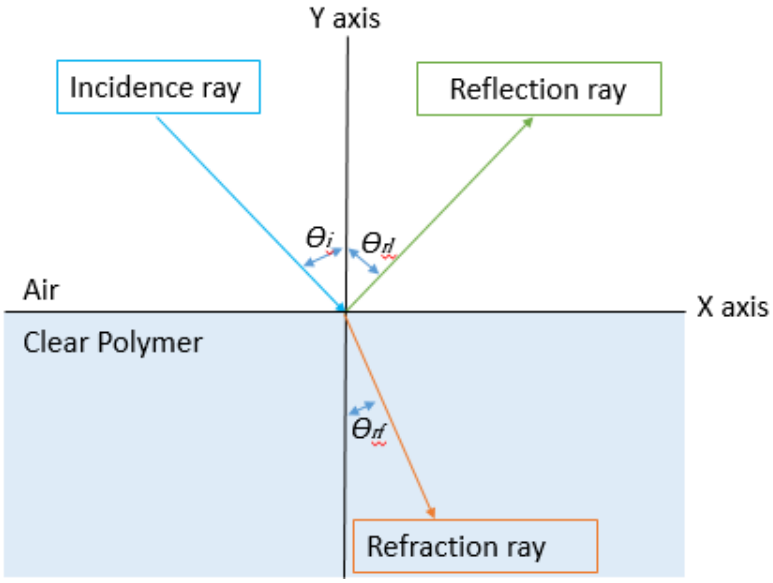

Figure 10 : Incidence Ray compared to Reflection Ray and Refraction Ray

Looking at Figure 10 the refraction array in orange, and the angle of refraction is *Θrf*. The angle of refraction can be determined by using Snell`s Law [26]:

$$\theta i = nr * \theta rf \qquad \textit{Equation 2}$$

Where:
Θi = angle of incidence
nr = index of refraction
Θrl = angle of refraction

2.5 Properties of sunlight

As the earth rotates around the sun, and around its own axis, there is a specific path the sun will follow. Furthermore, when traveling on earth there is another set of functions that must be observed. By using mathematical formulas, as well as geographical locations as to where the vehicle will be at a specific time, the optimal angle of incidence can be calculated.

2.5.1 Hour angle

The hour angles is to determine the angle the sun is moving through the sky according to the time of day. This converts the LST (Local Standard Time) into number of degrees, in which the sun moves across the sky.

$$HRA = 15(LST - 12) \qquad \textit{Equation 3}$$

As seen in the above equation, hour angle (HRA) is defined by 15° for each hour. This hour is LST – 12 for the 24H clock [27][28].

2.5.2 Declination angle

Where the hour angle uses time to determine the sun, the declination angle determines the tilt of the earth, depending on the number of days. Declination is the tilt of the earth on its axis as it rotates around the sun. This angle is north to south, relating to the perpendicular of the rotation around the sun [27][28].

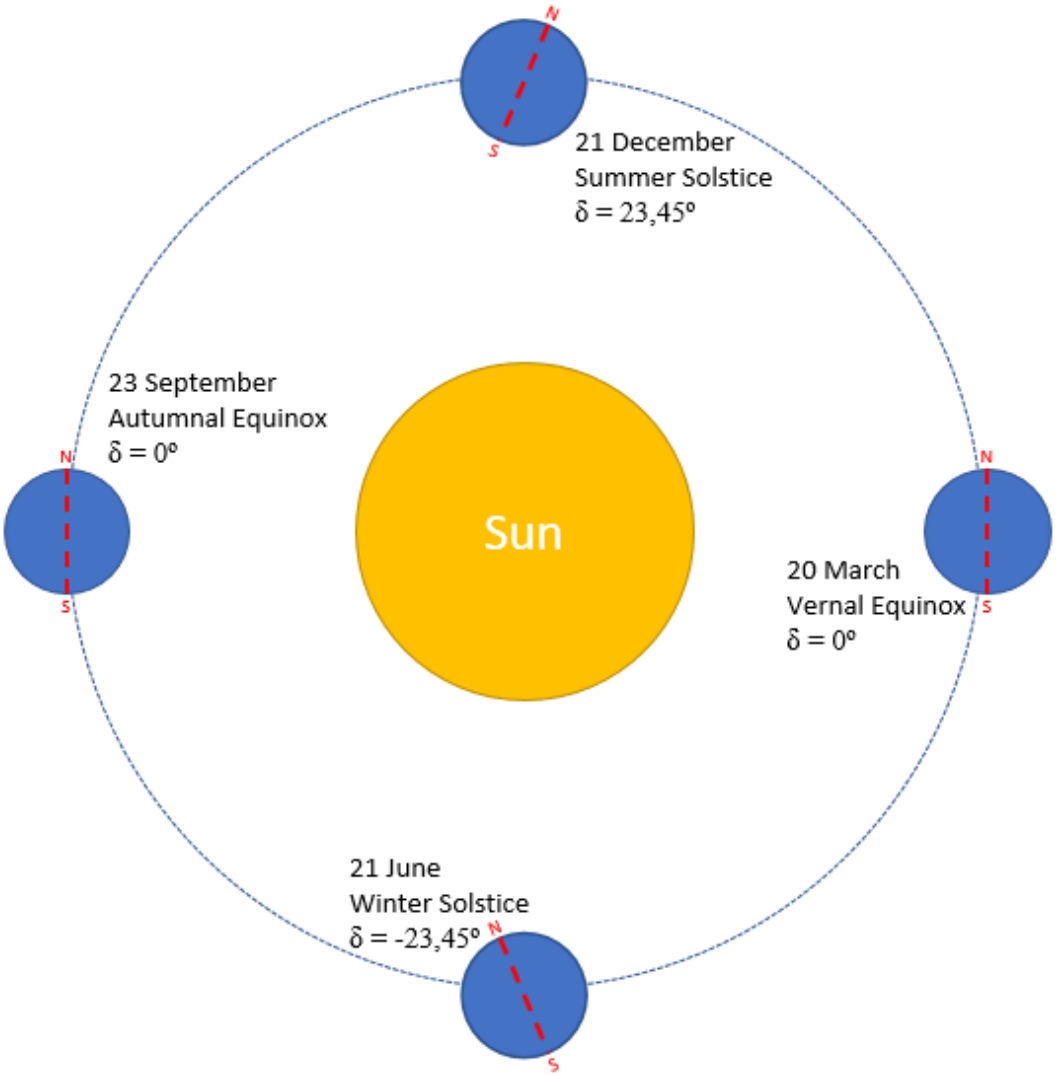

Figure 11 : Declination angle

Figure 11 depicts the way the earth tilts. There are four important dates to note, viz. 20 March and 23 September (vernal and autumnal equinox respectively), 21 December (summer solstice) and 21 June (winter solstice). At the summer solstice there are more hours in the day than at the winter solstice, which allows for longer days in summer [27][28].

$$\delta = -23.45° \times cos\left(\frac{360}{365} \times (d + 10)\right) \qquad \textit{Equation 4}$$

The above equation provides the answer to the angle of the declination angle. This is the maximum angle of winter solstice multiplied by the cosine of the decimal value of the day of the year.

2.5.3 Elevation angle

The elevation angle depends on the exact location on the earth in order to calculate the height of the sun at solar noon.

The angle of the height of the sun at sunrise from the horizontal line of latitude is 0°; on the equator at solar noon, it will be 90° (see the equation below).

$$\alpha = 90 + \varphi - \delta \qquad \textit{Equation 5}$$

$\alpha =$ *maximum elevation angle at solar noon*

$\varphi =$ latitude of the location

$\delta =$ declination Angle

$$\alpha = sin^{-1}(sin\delta \cdot sin\varphi + cos\delta \cdot cos\varphi \cdot cos(HRA)) \qquad \textit{Equation 6}$$

See the equation above for a more accurate representation of how to calculate the elevation angle [27][28].

2.5.4 Zenith angle

The zenith angle is the degree to which the solar module must be tilted from the flat position in order to acquire optimal surface area. The zenith angle can be calculated by using the declination and elevation angle in order to formulate the correct angle of incidence at which the rays of the sun will hit the earth.

The difference between the vertical line (perpendicular to the tangent of the equator) and the sun, is the extent to which the PV panels must be tilted away from the vertical in order to obtain the maximum amount of solar energy [29] [30].

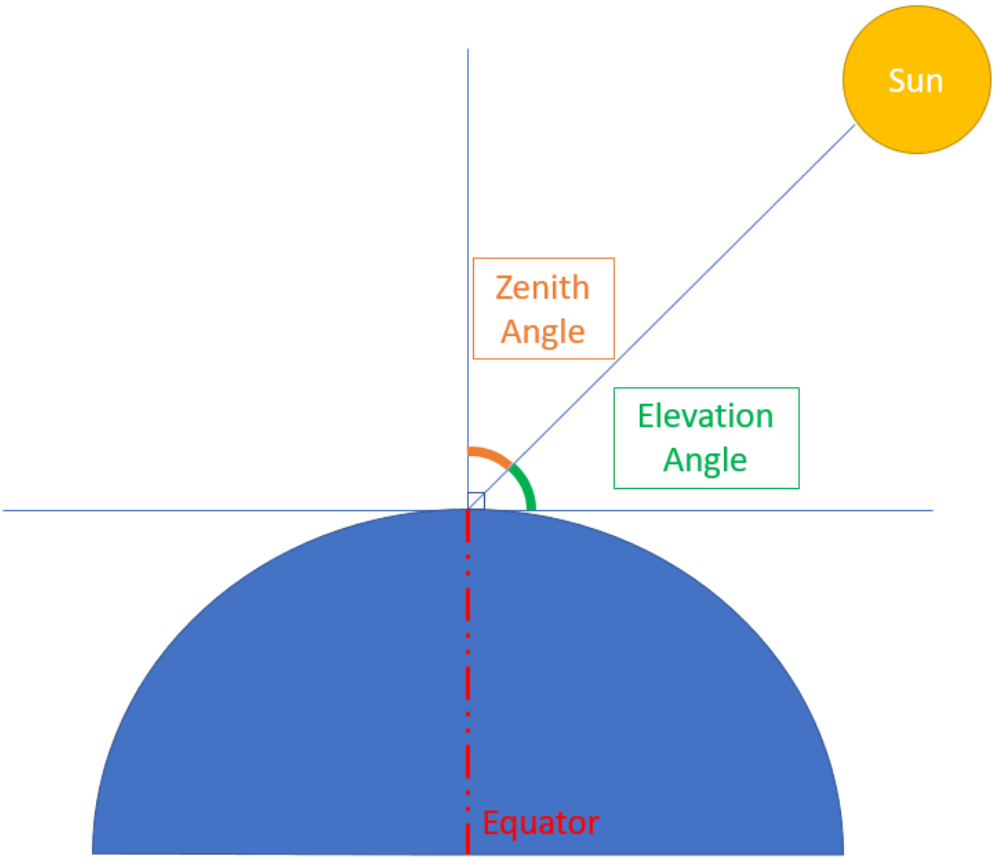

Figure 12 : Zenith angle and elevation angle

$\zeta = 90° - \alpha$ *Equation 7*

$\zeta =$ Zenith Angle

2.5.5 Azimuth Angle

Having the zenith angle to establish the height of the sun, the azimuth angle is needed to determine where the exact position of the sun will be. This is defined as the deviation angle from the north on a two-dimensional plane.

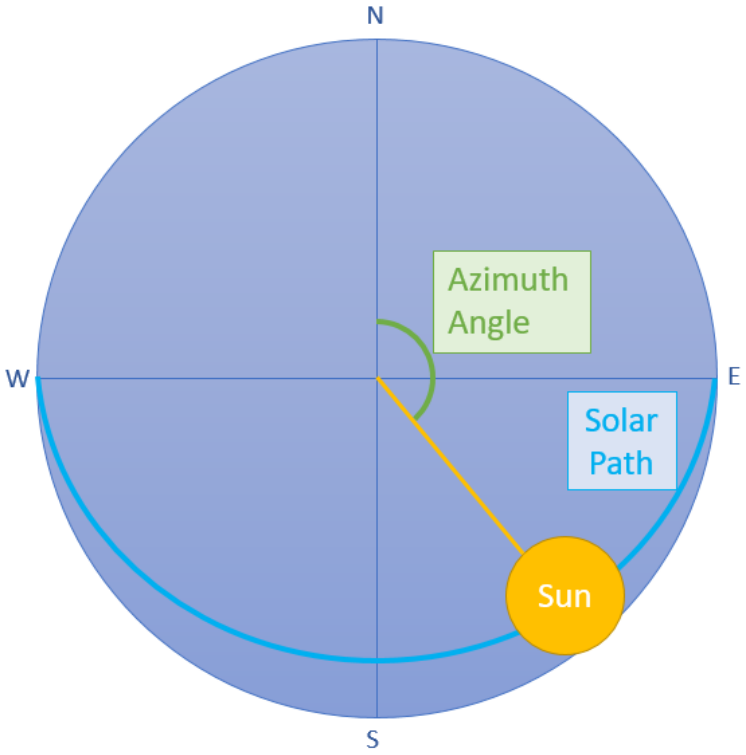

Figure 13 : Azimuth angle on the solar path

Although Figure 13 is two-dimensional, the solar path, when standing on earth is via the sky. The azimuth angle is the angle from north to the position of the sun [27][31].

$$Azimuth = cos^{-1}\left[\frac{sin\delta \cdot cos\varphi - cos\delta \cdot sin\varphi \cdot cos\,(HRA)}{cos\alpha}\right]$$ *Equation 8*

$\varphi =$ latitude

$\delta =$ declination

2.6 Components

Important factors to be considered in experiments regarding the evaluation of solar tracking for solar challenger race vehicles, are accuracy, reliability, and repeatability (test-retested reliability). The following hardware, components and algorithms are considered.

2.6.1 Arduino

The Arduino, is a low-level microcontroller having 8 bits and running at 16 MHz, will assist in repeatability by ensuring that each test is done using the same programmed parameters. This device is capable of acquiring up to 16 analogue values at nearly the same time by using multiplexing. Using open-source software, this device can be used to log directly into a PC [32].

Figure 14 : Arduino Mega [33]

Figure 14 depicts the Arduino Mega. The row of pins marked A0 – A15 is the analogue pins and is located to the right of the power pins.

2.6.2 Photodiode

The photodiode (PD) is a device used to determine the irradiation level of the sun, and measure how much power can be generated. A photodiode is a type of light detector that converts light into current or voltage. This device can operate in a number of modes:

• *Photovoltaic mode*. This is the zero-bias mode, in which the PD works similar a photovoltaic cell that produces a voltage when it is irradiated.

• *Photoconductive mode*. This is when the PD operates in reverse bias mode and turns into a current collector, rather than a voltage producer.

• *Avalanche diode mode*. This mode operates in a high reverse bias mode and is used to multiply the irradiation but is limited by the noise factor.

The BPW 34 is a type of photodiode that is commonly used. When connected in photovoltaic mode, it operates like a PV cell. This photodiode can be configured to measure solar irradiation as well [34].

Figure 15 : Photo op BPW 34 [23]

Figure 15 shows a BPW 34 photodiode.

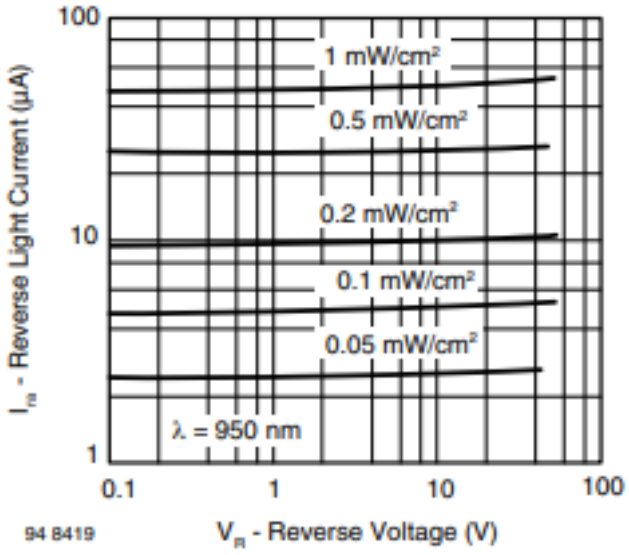

Figure 16 : Reverse light current vs Reverse voltage [23]

As seen in Figure 16, the reverse voltage is less affected by the irradiation than the reverse light current. This works to a similar principle as a PV module.

2.6.3 Halogen bulb

As a halogen bulb emits light at approximately the same wavelength and heat of solar irradiance, it can be used to simulate the sun on a very small scale [35][36]. It therefore is a suitable substitute for solar irradiance scale testing in a laboratory environment.

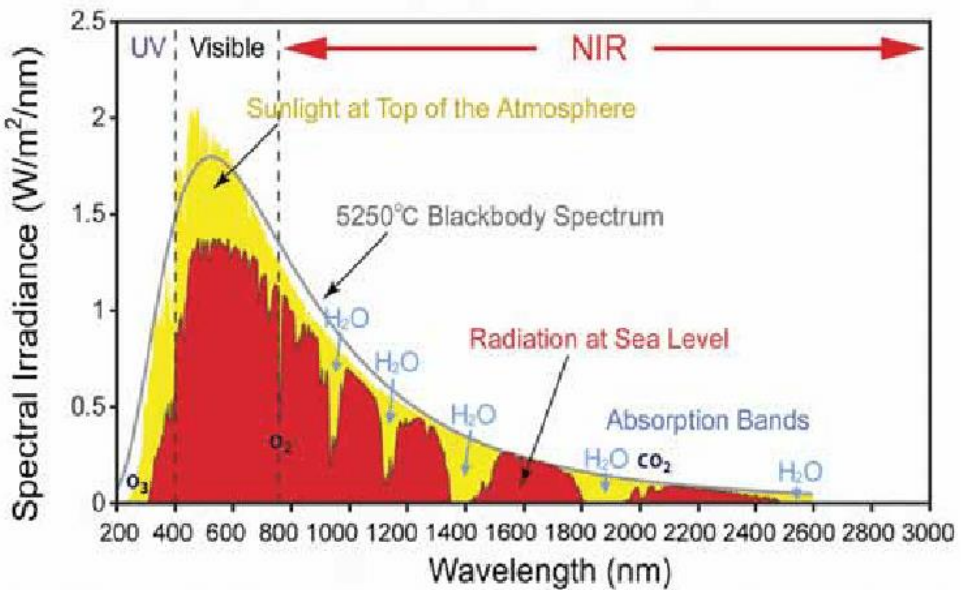

Figure 17 : Solar wave spectrum [37]

Figure 17 displays the sun's irradiation spectrum, i.e. the amount of light compared to the wavelength.

Figure 18 : Halogen bulb

Figure 18 is a photograph of a typical halogen bulb used to concentrate the power at a certain angle.

2.6.4 Pyranometer

A pyranometer, a device with a very small temperature coefficient, measures solar irradiation. [38].

Figure 19 : Pyranometer

A pyranometer suitable for this study, is the CMP 10 from Kipp & Zonen, displayed in Figure 19. The CMP 10 is known for its low thermal offset, fast response, and long there stability [39].

2.6.5 Buck circuit

A Buck circuit is traditionally used to step down a DC voltage and increase the current output. Thus, the voltage and current used by this circuit, if in the correct configuration, can be ideally controlled.

There is more than one possibility for S1 in Figure 20. A few common ones include the bipolar junction transistor (BJT), a current-controlled device that can handle high power, but the higher the current through the collector and emitter, the more current is required on the base. The metal oxide field-effect transistor (MOSFET) is a voltage-controlled device which is more effective when switching but is limited in voltage. Then there is the insulated gate bipolar transistor (IGBT), a MOSFET with BJT connected in a Darlington pair. The IGBT is a voltage-controlled device that can handle high currents similar to that of BJT. It does, however, require a MOSFET gate driver because of its capacitance in the gate.

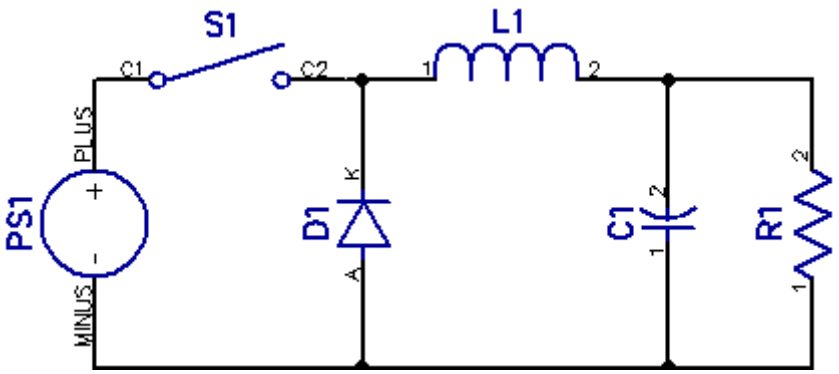

Figure 20 : Buck Converter circuit

In Figure 20 PS1 is the power source, and S1 is the switch controlled by a square wave generator to supply a duty cycle as is sensed over R1. C1 is charged when S1 is closed, with L1 restricting instantaneous change in current. When S1 opens, C1 discharges and the coil collapses in L1, with D1 regulating it to charge C1. Therefore, when measured over R1, there is a nearly constant voltage.

2.6.6 Maximum Power Point Tracker

The maximum power point tracker operates at the maximum power point, or MPP. A photovoltaic cell can be divided into two states of operation, viz. short circuit, and open circuit. Short circuit is when the voltage drops to close to zero and the current is maximum. The same principle is true for open circuit, but the closer to zero the current is drawn, the higher the voltage will be. At a specific but changing point, the voltage and current drawn will produce the maximum power. This change is due to weather, dust, or other factors. Thus, the MPPT always attempts to keep the power dawn from the module at the maximum power point.

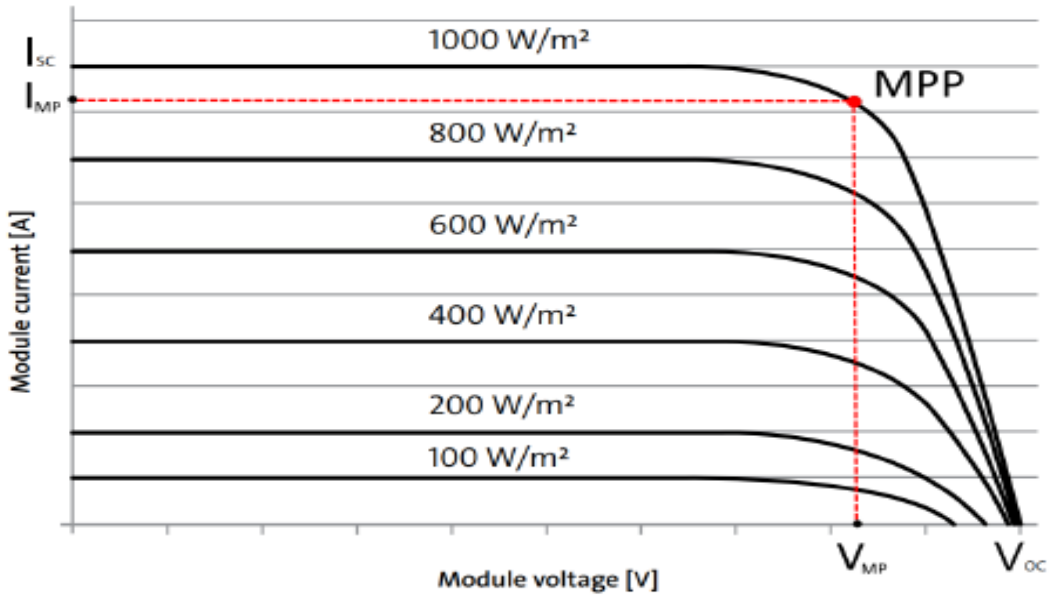

Figure 21 : Maximum power point

In Figure 21 Isc represents the short-circuit current, Imp the maximum power point current, Voc the open-circuit voltage, and Vmp the maximum power point voltage. Figure 21 is a standard IV curve of a PV module at standard test conditions (STC). As observed in the IV curve, moving in either direction of the MPP will have a drastic loss in power output.

With the varying irradiation of W/m², the IV curve subsequently moves the MPP. It is critical to maintaining maximum power output.

There are various MPPT algorithms, namely:

- Constant voltage (CV): CV is the simplest technique, as it uses a set voltage that is pre-programmed according to the specifications of the module and then sticks to that voltage. This method ignores current, irradiation and temperature; it only concentrates on voltage. This also is the reason why the tracking almost never is on the MPP.

- Short-current pulse (SC): The SC method controls the converter by obtaining the short-circuit current (Isc) of the module, and then compares it to a pre-programmed reference current (Iref). After the comparison, it will adjust the PWM of the DC/DC converter.

- Open voltage (OV): OV is similar to the SC method, but instead of short-circuiting, this method will go into open-circuit to obtain the module open voltage (Voc). The maximum power voltage (Vmp) is close to 76% of the open voltage (Voc).

- Perturb & Observe (P&O): The P&O method operates by periodically perturbing the PWM duty cycle of the DC/DC converter. The resulting power is then compared to the previous power value, and a decision is made to increment or decrement the duty cycle.

- Incremental conductance (IC): Incremental conductance is based on the observation that follows Equation 3 to hold the MPP.

$$\Delta_{mpp} = \frac{\Delta I_{pv}}{\Delta V_{pv}} + \frac{I_{pv}}{V_{pv}} = 0$$

I_{pv} and V_{pv} denote the current and voltage of the PV module with

$$\Delta V_{pv} = V_{pv}(n) - V_{pv}(n-1)$$

and

$$\Delta I_{pv} = I_{pv}(n) - I_{pv}(n-1)$$

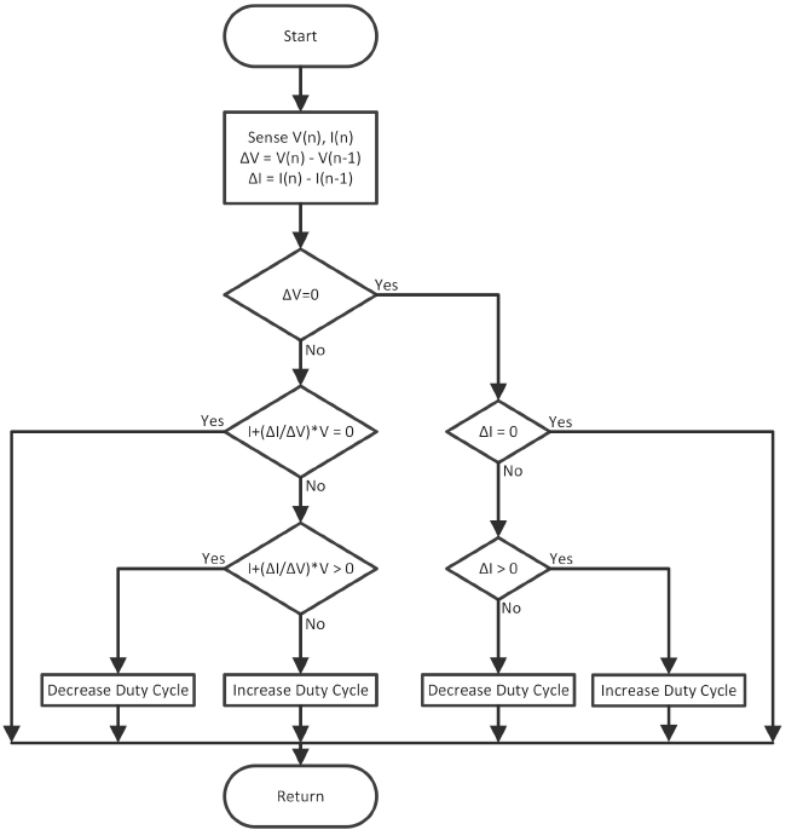

Figure 22 : Incremental Conductance flowchart

Operation of the PV module on the IV curve as in Figure 21 is relative to Equation 3 and can be explained as follows: When Δmpp > 0, the module is operating at a power point Pp to the left of the ideal MPP, and when Δmpp < 0 the Pp is to the right of the MPP. This IC variant of the MPPT algorithm is ideal for rapidly changing atmospheric conditions and therefore our selected method for implementation. Figure 22 above shows the flow diagram of the IC algorithm for tracking the MPP.

2.7 Concluding remarks

In this chapter the literature demonstrates that the Solar Challenge is of importance to the development of solar vehicle technology. It shows that the Solar Challenge is an international challenge involving international competitive teams with large sponsorship opportunities. The need for solar tracking evaluation would therefore be beneficial for such a challenge. Literature confirms that solar generation is a viable option for South Africa. Literature was evaluated to identify the optimal cover material for solar tracking, with poly carbonate showing strength and transparency.

Theories of light transmission obstacles showed that light behave in different manners in different media, it's important to note that properties of light one must consider the angle of incidence to the panel relative to the position of the sun on different positions on the globe, that influences solar tracking and power generation. Components needed for the instrument development is discussed and includes microcontrollers such as an Arduino and different types of sensors. MPPT will be mandatory for test because it must control the power drain from the panel to the utmost ideal power generation, this will be crucial in design and construction for test instrumentation.

Chapter 3: Methods and techniques

Chapter 3 demonstrates methods for solar tracking evaluation and comparison towards a competitive solar challenger race vehicle. This includes the evaluation and comparison of solar tracking with and without an aerodynamic dome. This would lead to discussions on what should influence performance considerations for competitiveness. The transparent materials suggested by the literature should be used to construct an aerodynamically shaped dome to minimise drag but still give acceptable irradiation transfer for power generation. These sections show the design of a scale instrument to measure power generation at different inclinations for cover materials parameters. Finally, it demonstrates and explains a scientific method of evaluation and comparison of solar tracking on the actual solar challenger vehicle. Chapter 3 demonstrates how to generate, analyse and present the results for discussion.

3.1 Comparison of cover material

The literature review evaluated five possible solutions for PV cover material selection. The table below is proposed for comparing the different materials. The table shows the different characteristics of each material. This comparison should result in the optimal solution to what polymer will be best for the cover material.

Table 1 : Material table that will be used to compare characteristics from materials before it is populated.

	Unit	Material 1	Material 2	Material 3	Material 4	Material 5
Density	g*cm^3					
Tensile Strength to breaking	MPa					
Elongation to Breaking	%					
Light Transmission	%					
Refractive Index	%					

Density, as in its name, determines the weight of the material in the final product – a critical factor. With weight directly related to power, a lighter vehicle would require less power, whereas a heavy vehicle will require substantially more power.

Tensile strength to breaking determines the possibility of the material breaking during blunt impact force. Failure point will be when the blunt object penetrates the material, evidently depending on the mass of the material. The tensile strength is critical, since the driver relies on this material to protect him from an oncoming object, e.g. a rock thrown up by a truck.

Elongation to breaking determines how far the material will stretch before it breaks. This percentage is an indication to how long and strong the chemical bonds are, and an indication of whether the material will shatter or shear when an object penetrates it. When the material shatters, it can injure the driver, but when it shears it can slow down the object that leads to a lesser injury.

Light transmission is how much of the light spectrum will be able to pass through the material. This is important for allowing the correct spectrum through, as well as enough of that spectrum, so that there is the minimal loss of light through the cover to the PV module.

In the literature review 2.4.2 the refractive index explains how the light will bend. When the light is refracted at an obscure angle, it will cause too much light will be lost and as stated, the ideal is to strive towards minimum loss of light and maximum power generation.

3.2 Scale-model evaluation method

This section demonstrates the design of a testing instrument, as well as a test method, to evaluate transparent cover materials

3.2.1 Experimental Setup

The instrument is constructed with a halogen bulb that has similar properties to that of the sun, as seen in literature review 2.6.3. The instrument should have the ability to measure the irradiation loss. The BPW34 is chosen, as it is a photodiode that operates similarly to that of a PV module (see literature review 2.6.2) to do the test, and to determine the irradiation that is generated. All raw data is logged onto a PC for further analysis via serial communication with Arduino (explained in literature review 2.6.1).

Observe the proposed physical operation in Figure 23. The instrument should be constructed with an array of BPW34 photodiodes (PDs). A halogen bulb is motorised on an axis to simulate a similar path to that of the sun at solar noon. The halogen bulb has substantially less power, as it must be closer to the PD. Measurement is calibrated and verified by using a pyrometer.

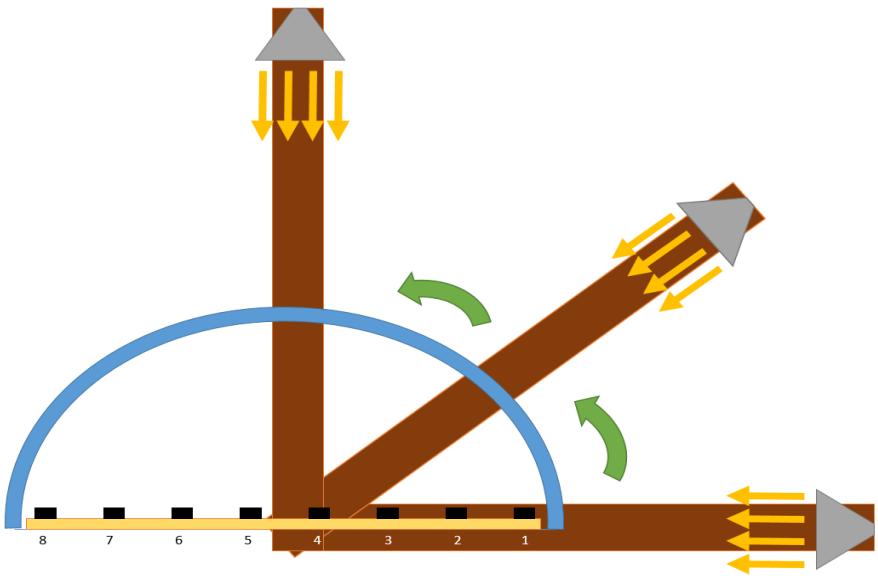

Figure 23 : Rotation of arm on the scale-model test

Figure 23 shows a sketch of the angular movement. The instrument must simulate the course of the sun, rising from one side and following through.

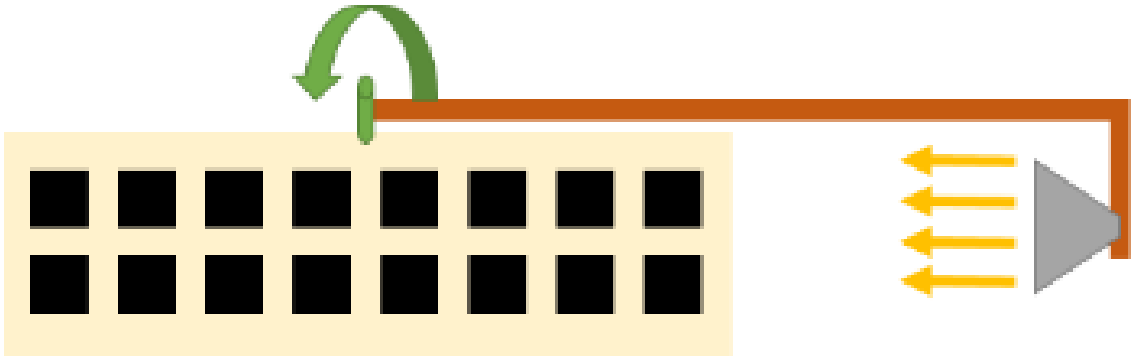

Figure 24 : Placement of the PD on the scale-model test

Figure 24 above shows a halogen light source that can rotate over the PDs seen as the black squares. Note that they are configured in pairs through rows 1-8 starting on the left. The data acquisition is done using an Arduino that captures the ADC values to a computer.

Figure 25 : The scale-model test station after construction

Observe the real-world construction of the instrument in Figure 25. The light, PD and Arduino are clearly visible.

The measurement circuitry consists of light sensors connected to the analogue inputs of an Arduino. From the Arduino the data is logged to a PC for further processing.

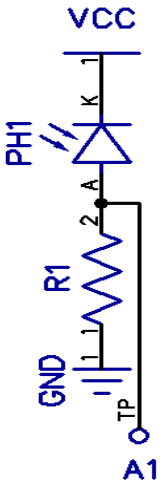

Figure 26 : Diagram showing how to connect the PD

Figure 26 is the typical connection diagram of how the BPW is connected, in order to allow for a larger voltage difference as the irradiation increases. By considering Figure 16 and taking Ohm's law into consideration, R1 in Figure 26 stays constant, but varying irradiation will cause a small change in the current flowing through the circuit. This allows for a higher step-up ratio between the irradiation and the ADC value from the Arduino which is a 10-bit analogue to digital converter. Through the use of quantisation, i.e. the voltage per division, the input of the data set will be constrained. This process takes a large number of readings and produces an output that is smaller but also accurate. But this means that there is 0 – 5 V that is divided into 0 – 1 023. Therefore 5V over 1024 bits equates to 4.9 mV per unit. Averaging was achieved by sampling at a higher than needed Nyquist frequency and running it through the finite impulse response filter.

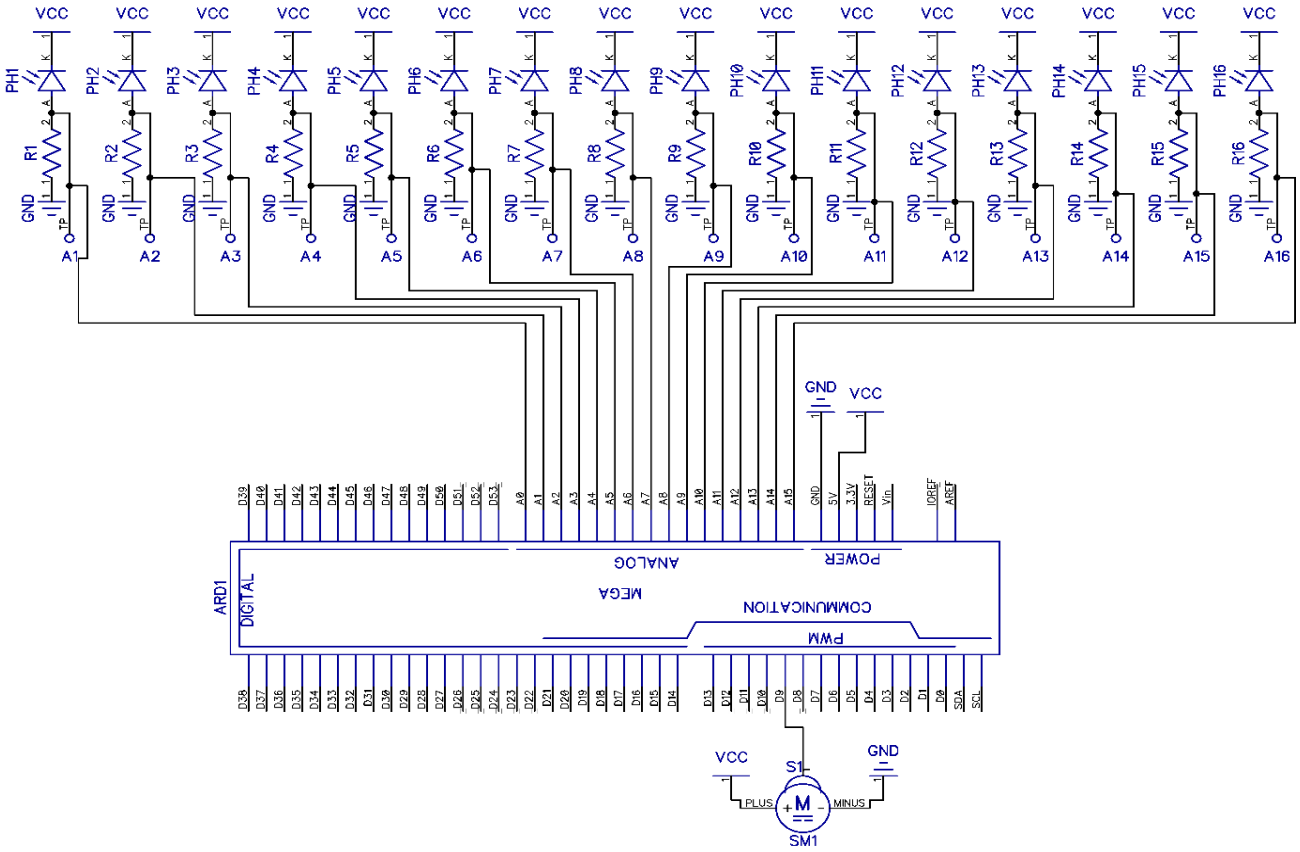

Figure 27 : Diagram of the scale-model test

Create an array of sensors for more accurate data by taking the diagram in Figure 26 and adding 16 of them to the 16 ADC pins on the Arduino Mega. Then use the same microcontroller to drive the servomotor as seen in Figure 27 above.

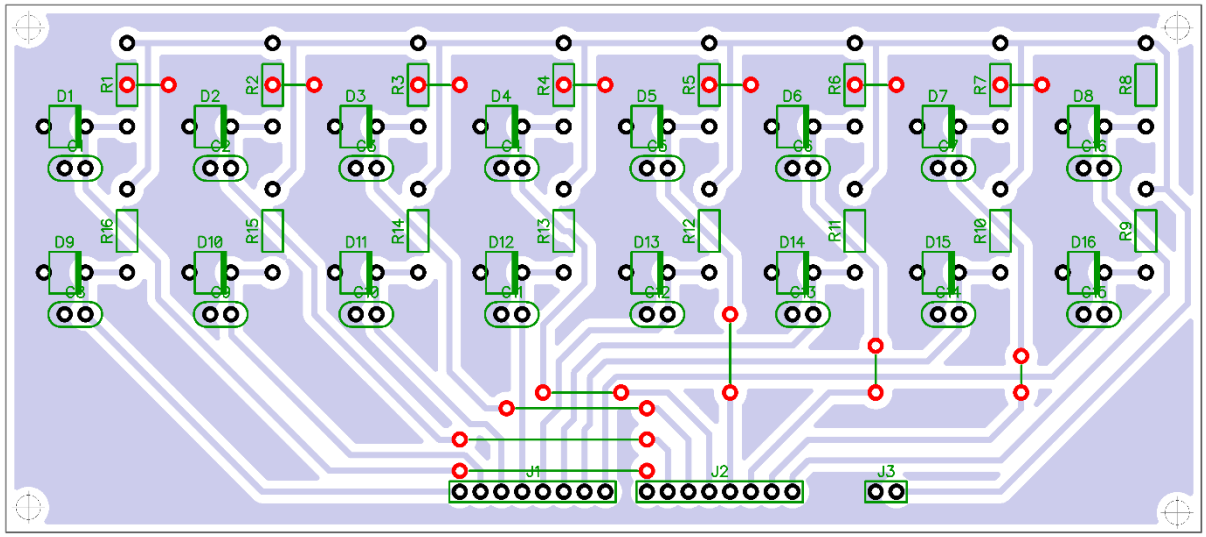

Figure 28 : Artwork of the printed circuit board (PCB) for scale-model test

Figure 28 is the artwork for the PCB, and is based on the diagram in Figure 27, and will fit onto the Arduino Mega.

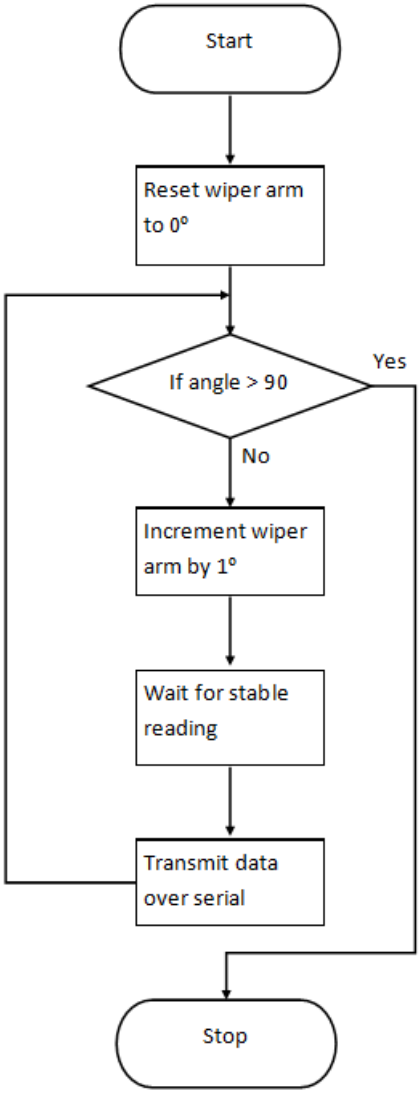

Figure 29 : Flowchart of how the scale-model test will operate

With hardware described in Figure 27, the software uses the flowchart in Figure 29. Note that the actuator arm is reset to 0°. First, test if the actuator arm is more than 90°; the test from 0° – 90° has an isometric shape and will have similar readings for 90° – 180°. If the actuator arm is set at less than 90°, it will start by incrementing the actuator arm by one degree, and then take readings every 50 ms. Only when five consecutive readings are the same, it will it send the data through to the serial

monitor for further analysis. With the first cycle complete, it will continue until it reaches the desired 90° and then stop.

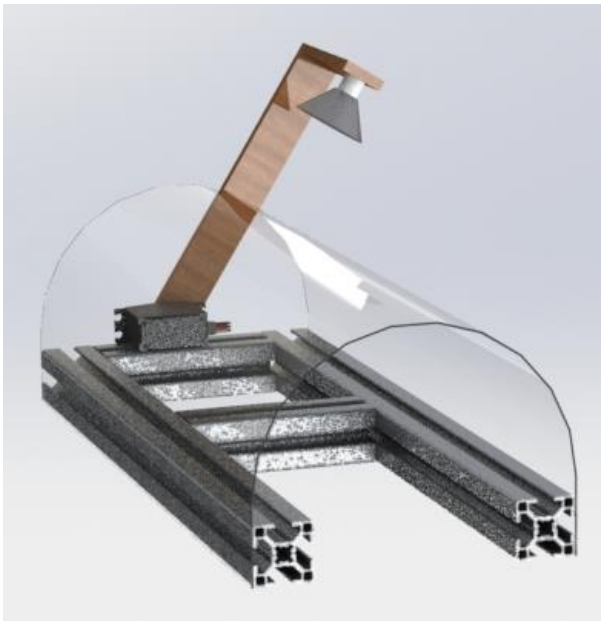

Figure 30 : CAD of the scale-model test

Figure 30 is the CAD used to build the scale model. This CAD model was designed using Solid Works.

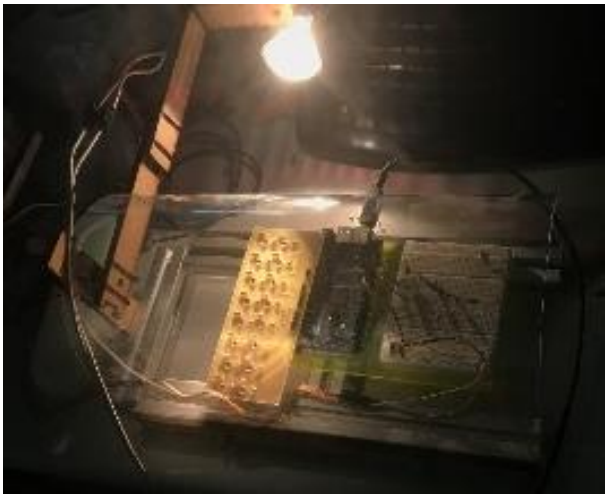

Figure 31 : the scale-model test in operation with the cover on

Figure 31 shows the constructed instrument, as constructed from the planning phase in Figure 23 and Figure 24 that was digitize to the CAD in Figure 30. A halogen bulb is motorised by means of Arduino and a servomotor to move over the diodes while increasing the degrees about the

horizontal level to simulate the sun. The halogen bulb is programmed to move one degree at a time, stop to stabilise, take measurements of irradiance one row at a time, and then repeat. This is done to 90°, as the shape of the PC cover is symmetrical and therefore the data will be a mirror image about the 90° vertex.

Figure 31 shows a side view of the test. Note that the change in degrees of the light sources will be increased through each step, stating at 0° up to 90°.

Figure 32 : The scale-model test in operation without the cover

Figure 32 shows the test without any cover material. The PD can be seen with the light at 90° degrees to the PDs. In Figure 31 showing the test with the cover material on, the reflection of the light is clearly visible, as is a shading. Note that the cover material is setup convexly to measure incidence losses. The test is conducted in a darkroom at 25 °C.

Samples are taken at each interval and logged to a spreadsheet. All the raw data is pushed into a comma-delimited file. The data is then imported to Excel where it is converted from the ACD value to Wattage per metre square (W/m^2). In order to convert the raw data into useful information, the raw data will be compared to readings from the CMP10 pyranometer, after which a scale factor will be calculated to conform with the data. As both the PD and pyranometer have a linear increase, the slope can be determined and then used to calculate the scale factor. Since this test will be repeated multiple times, the data will be averaged and then only it will be converted to irradiation. After

irradiation is calculated, it will be exported to MATLAB for the graphs to be drawn. The graphs cover the data generated from this experiment and will compare each column individually. This will show the difference between cover and 'no cover', Wattage per metre squared for the Y-axis, and the degree on the X-axis.

3.2.2 Calibration

In order to obtain accurate data, each sensor of the scale model must be calibrated prior to testing. Data obtained is similar under standard test conditions (STC). This data is compared to a pyranometer that will be used in the CMP10 from Kipp & Zonen to calibrate the W/m², as was explained in Section 2.6.4. Each of the sensors is connected individually and compared to the pyranometer, and then calibrated accordingly. The measurement from the pyranometer will be used in a stand-alone device which displays the real-time irradiation.

3.3 Panel layout

As solar cells are connected in series to form a solar module, the whole module goes down if one cell goes down. Consequently, when one cell is shaded the whole string is compromised. A possible solution for this is the bypass diodes, which are quite expensive.

Results from the scaled experiment, as well as the physical design of the vehicle, would determine bypass diode placement.

The tilting panel layout is as follows. The bottom part of the vehicle can be seen in the figure below.

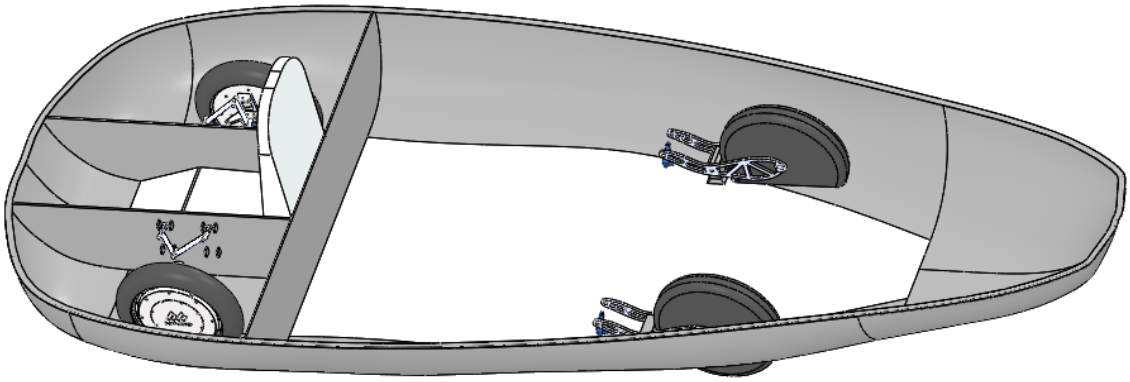

Figure 33 : Bottom part of the solar vehicle

To the right of Figure 33 is the front part of the vehicle. The two front wheels are the in-hub motors. The cavity behind the driver and around the back wheels is where the movable panels are placed.

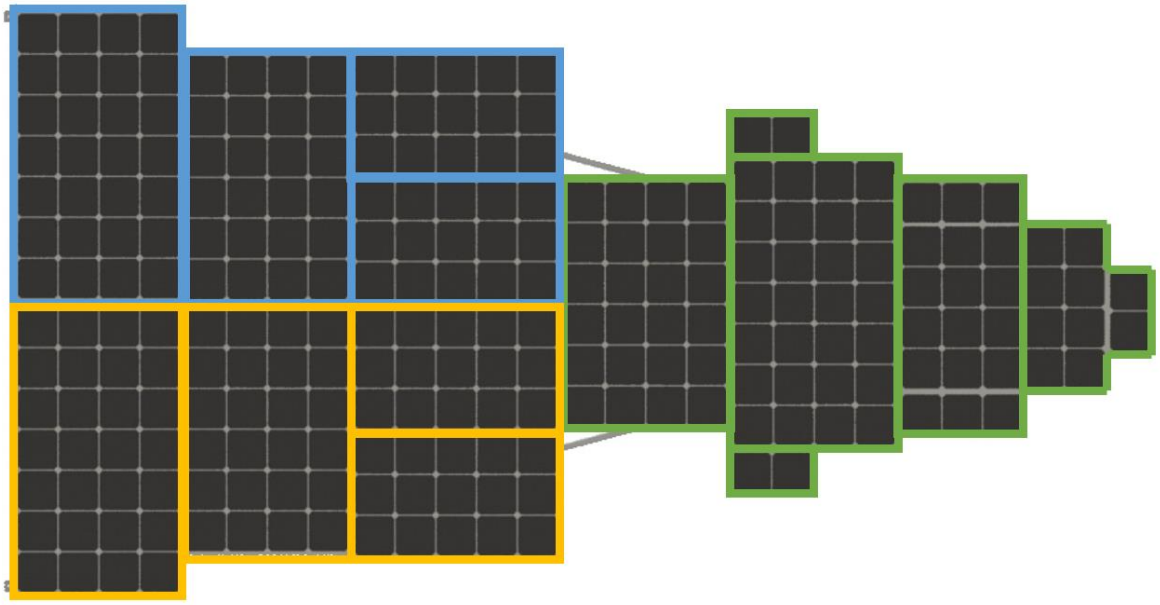

Figure 34 : PV layout of strings

The complete module is wired up into three strings of approximately the same size as indicated with blue, orange and green. Each block is wired in series. Consequently, if one of the blocks underperforms, the entire string will be underperforming. The bypass diodes must be placed in such a way as to bypass the underperforming cells. The placement is further discussed is discussed in Section 4.2.

3.4 Full-scale evaluation method

This section demonstrates the solar tracking evaluation and comparison method for the full-scale solar challenge vehicle. In order to evaluate the full scale a few aspects must be considered: the environment, the PV module stress test instrument and the logging table.

3.4.1 Environment

Effective measurement of the vehicle's power generation requires a designated area enabling 360° rotation and ample space to gather data at various intervals, with and without cover material.

Figure 35 : Map of the campus

In Figure 35 the red X marks the designated testing area. It offers a clear view of the sky and an unrestricted view of the sun from 07:00 – 17:00, as stipulated in the Sasol Solar Challenge rules.

Figure 36 : Solar Vehicle test

Figure 36 shows the vehicle at the area designated for the experiment, with cover material on and test equipment to the front.

3.4.2 PV module Stress test instrument

Stress testing of the PV Module is to run the module at maximum power and dissipating all the energy. This is to compare the difference between varying models, as well as between different modules from the same manufacturer and the same size.

An instrument has been developed to conduct stress testing. This device uses an active load to simulate a depleted battery to draw maximum power from the module. As seen in Figure 21 (Section 2.6.6), there is an optimal point on the IV curve. When only the current is taken into consideration, it will result in a short circuit and the volts will drop, but the current withdrawn will not

increase past Isc. The same applies to open-circuit voltage; when volts are too high the loss in current will produce sub-optimal power. This controller follows the incremental conductance IC as explained in (Section 2.6.6). This is a fast response algorithm that can quickly adjust to the performance of the PV module.

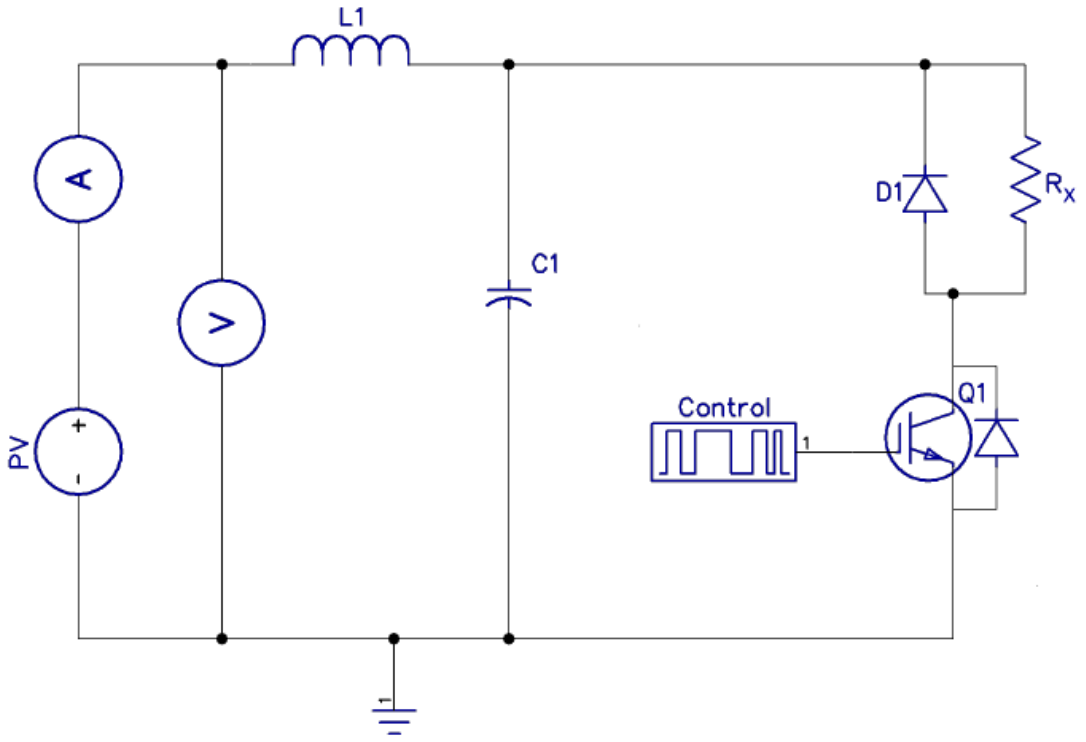

Figure 37 : Power electronic circuit to stimulate panels to operate at MPP, and dissipate all energy into heat.

The above diagram (Figure 37) depicts an electronic power circuit performing an energy transfer. It converts the electrical power into heat power. The PV module is an energy source with Q1 as the power switch to vary the conduction through the fixed resistor Rx. L1 and C1 form a low-pass filter to minimise the switching effect on the solar panel, thus allowing a relatively constant current.

R1 in Figure 37 absorbs the total power of the PV module. Due to the high-power requirement, the resistors must be wire-wound. Wire-wound resistors act as inductors when switched on. D1 is therefore added to discharge the energy stored during the off time of the duty cycle.

Rx must be determined in the setup process. This is done by utilising the IV curve. The duty cycle of the PWM has an effective range of 0,1 – 0,9. This there is responsible for a large range of variable resistance. By varying the resistance, the current remains proportional, thus enabling the operational power point to follow the IV curve to achieve MPP.

3.4.3 Experimentation data Table

The official route as seen in Figure 38 travels in a southerly direction for a large part of the route. Then it turns towards the west, although Figure 38 does not display the daily route and, more specifically, the daily loops. Therefore, the angle incidence at which the sun will hit the panels, can be accurately predicted. Since travel time is between 08:00 and 17:00, the angle of incidence can be from different angles as the vehicle moves around the daily loop. The angle of incidence can be adjusted in advance and the panels set accordingly; this would also help to get the best angles through mountain passes. As explained in Section 2.5, the solar angle can be predicted accurately by utilising longitude and latitude combined with the time of day. Then, since the angle of incidence is known, the co-ordinates can be calculated of where exactly the vehicle will be receptive to the predicted speed. However, as mentioned in Section 4.1, each material has its own refractive index, and in Section 2.4 reflection comes with refraction. The model in Section 3.2 was designed to obtain data on the number of losses that can be expected.

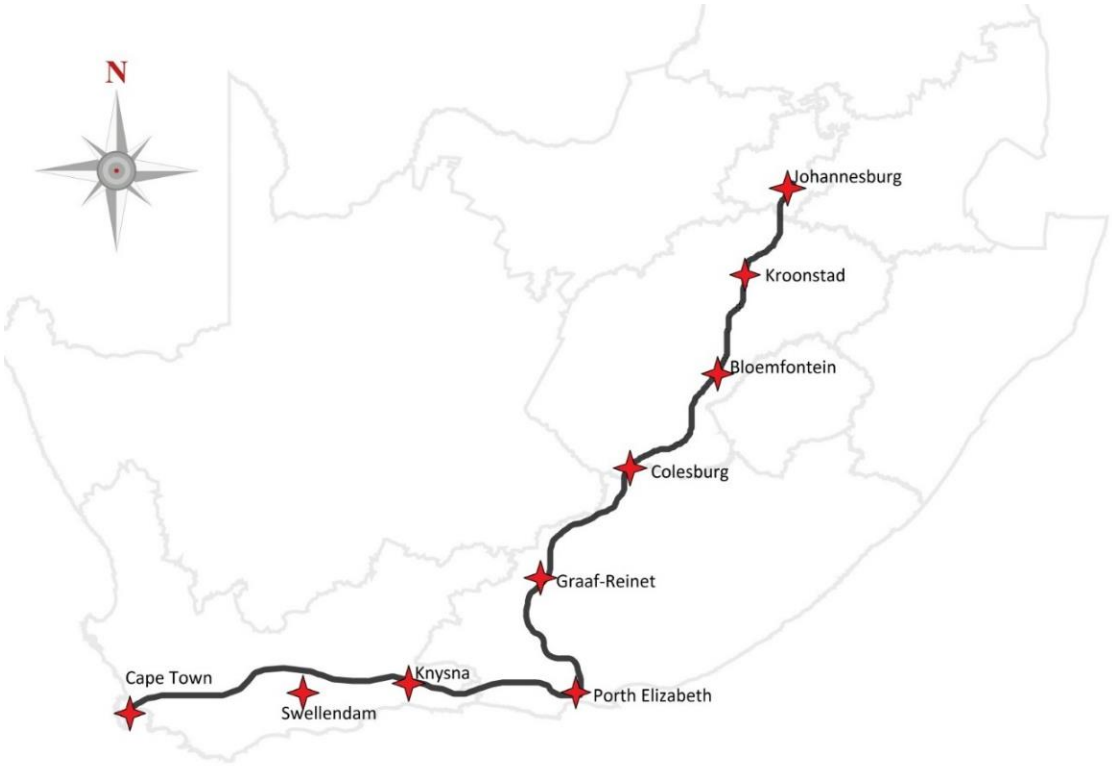

Figure 38 : The 2018 official route

The following table has been developed to evaluate the performance of the vehicle, with Table 2 showing a zoom in section of the full table displayed in Table 3

The table below shows the voltage and current at different time intervals, at different angles, and with and without cover.

Table 2 : This table will be used to do data acquisition, but it is a zoomed in version, showing only one data set.

Time	Irradiation	Direction	Flat Cover									
			Voltage 1	Current 1	Watts 1	Voltage 2	Current 2	Watts 2	Voltage 3	Current 3	Watts 3	Total Watts
07:00		East										
		South										
		West										
		North										
08:00		East										
		South										
		West										
		North										
09:00		East										
		South										
		West										
		North										
10:00		East										
		South										
		West										
		North										
11:00		East										
		South										
		West										
		North										
12:00		East										
		South										
		West										
		North										
13:00		East										
		South										
		West										
		North										
14:00		East										
		South										
		West										
		North										
15:00		East										
		South										
		West										
		North										
16:00		East										
		South										
		West										
		North										
17:00		East										
		South										
		West										
		North										

Table 3 : This table will be used to do data acquisition, but it is a zoomed in version, showing all four data sets.

Time	Irradiation	Direction	Flat Cover										Flat No Cover									
			Voltage 1	Current 1	Watts 1	Voltage 2	Current 2	Watts 2	Voltage 3	Current 3	Watts 3	Total Watts	Voltage 1	Current 1	Watts 1	Voltage 2	Current 2	Watts 2	Voltage 3	Current 3	Watts 3	Total Watts
07:00		East																				
		South																				
		West																				
		North																				
08:00		East																				
		South																				
		West																				
		North																				
09:00		East																				
		South																				
		West																				
		North																				
10:00		East																				
		South																				
		West																				
		North																				
11:00		East																				
		South																				
		West																				
		North																				
12:00		East																				
		South																				
		West																				
		North																				
13:00		East																				
		South																				
		West																				
		North																				
14:00		East																				
		South																				
		West																				
		North																				
15:00		East																				
		South																				
		West																				
		North																				
16:00		East																				
		South																				
		West																				
		North																				
17:00		East																				
		South																				
		West																				
		North																				

Time	Irradiation	Direction	Tilted Cover										Tilted No Cover									
			Voltage 1	Current 1	Watts 1	Voltage 2	Current 2	Watts 2	Voltage 3	Current 3	Watts 3	Total Watts	Voltage 1	Current 1	Watts 1	Voltage 2	Current 2	Watts 2	Voltage 3	Current 3	Watts 3	Total Watts
07:00		East																				
		South																				
		West																				
		North																				
08:00		East																				
		South																				
		West																				
		North																				
09:00		East																				
		South																				
		West																				
		North																				
10:00		East																				
		South																				
		West																				
		North																				
11:00		East																				
		South																				
		West																				
		North																				
12:00		East																				
		South																				
		West																				
		North																				
13:00		East																				
		South																				
		West																				
		North																				
14:00		East																				
		South																				
		West																				
		North																				
15:00		East																				
		South																				
		West																				
		North																				
16:00		East																				
		South																				
		West																				
		North																				
17:00		East																				
		South																				
		West																				
		North																				

The test instrument is a DC-DC converter running on a fast response algorithm like that of incremental conductance.

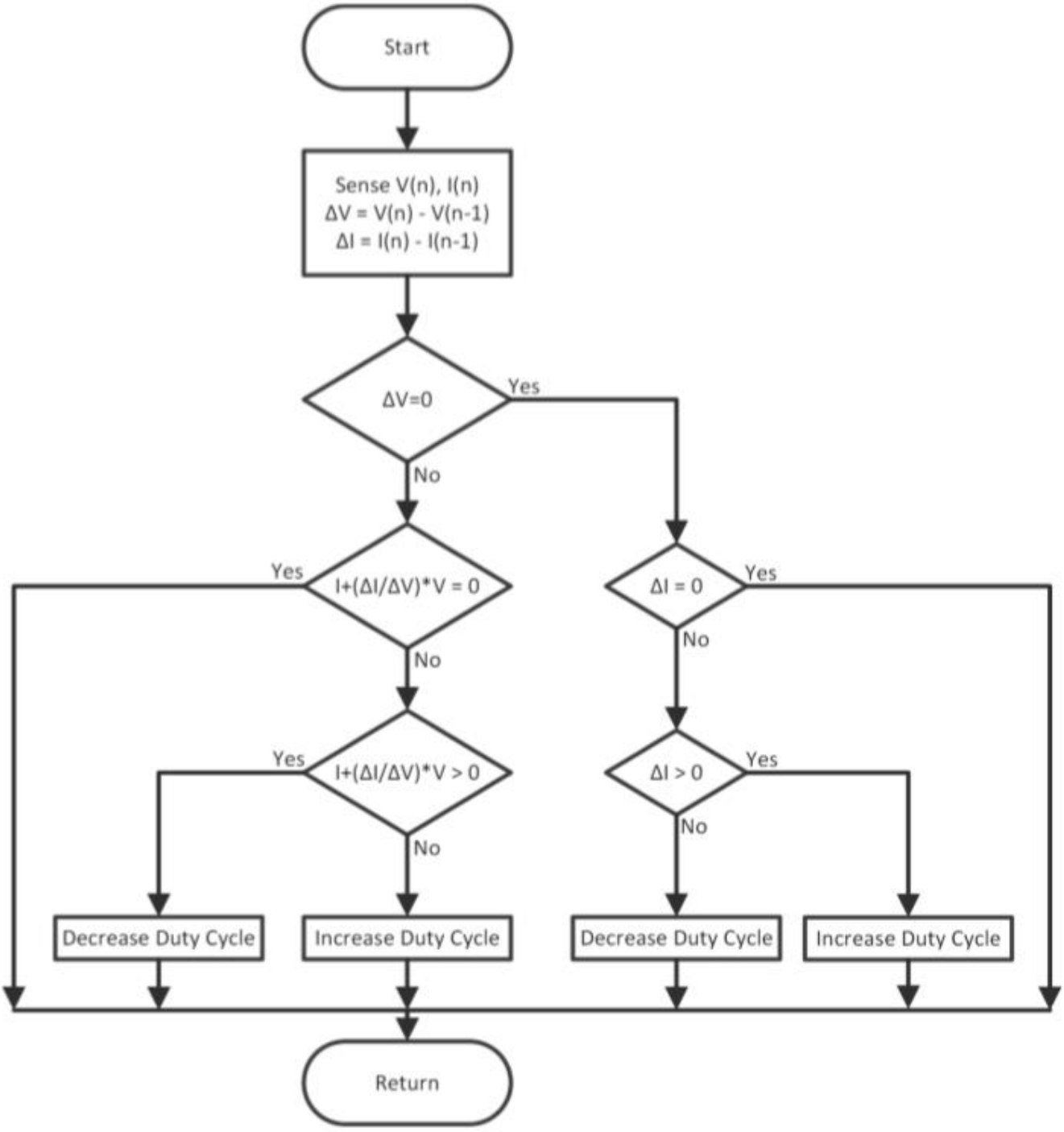

Figure 39 : IC algorithm flowchart

Figure 39 above shows the flow diagram. At the start of the cycle, the software takes a reading of what is happening in the circuit and compares it to the previous reading to find the change in the

parameters. Step one in the algorithm is to determine whether there was a voltage difference; if not, then whether there was a current difference; if not, then there is no change. If there was a change in current, it would be a positive or negative change and adjust the duty cycle accordingly. If there was a voltage difference, the microcontroller must do a quick calculation to determine the correct path through the IC algorithm.

The total power generation of panels on the solar vehicle is 980W for 4 m². This was then divided into three approximately similar strings comprising 300W, 340W and 340W. All three were individually controlled to ensure optimal power conditions. The setup was mounted onto the solar vehicle with a tilt system for generating precise and repeatable results.

Each test was performed hourly with the cover on and off, and at four orientations and two tilt levels. This means that every hour the measurements were taken with the tail of the vehicle pointing north, the panels flat, and the cover off. Then, next the panels were tilted and the measurements taken again. Then the cover was placed back on the vehicle and the process repeated. Then the orientation was changed so that that the tail end faced east, and the measuring process repeated. The entire process was repeated until all four directions were covered with all four tests done at each point is. Then the results table was populated.

3.5 Concluding remarks

In this chapter the different methods that produce scientifically based solar tracking evaluation results were discussed. These solar tracking evaluation methods include the comparison of several factors of cover materials, including weight, safety, and light transmission. Scaled methods should show how to develop a platform for small-scale testing with grid testing, as each photo diode is individually monitored. Full-scale evaluation methods show how to evaluate the panels on performance with tracking. This involves stress testing the solar panels in different directions or orientations to represent directions followed by the solar challenge.

Chapter 4: Results

Chapter 4 discusses the results for the solar tracking evaluation and comparison towards a competitive solar challenger race vehicle. This includes the results for the optimal material for the design and construction of a transparent, aerodynamic dome under which tracking is possible, as well as evaluating the power losses for a discussion on this versus the aerodynamic gains of improved drag. In this section the cover materials (as suggested by the literature) are compared, motivating the selected one. Thereafter the optimal selected material is evaluated with the designed scale instrument, the design and construction of which are shown in Chapter 3. The data, as presented in Chapter 3, is extracted, analysed, and discussed. This section will demonstrate and discuss how these results, among other factors, influenced bypass diode placements for optimal power generation. Finally, the actual solar challenger vehicle measurements of tracking, non-tracking with and without cover are taken, as explained in Section 3.4.

4.1 Literature review comparison of cover material results

The proposed table from Section 3.1 below is populated with the different types of polymers. These are compared in the table below to select the optimal solution

Table 4 : Cover material comparison of possible solutions to the correct cover material.

	Unit	PET	PC	PMMA	SAN	PS
Density	g*cm^3	1,34	1,2	1,19	1,08	1,05
Tensile Strength to breaking	MPa	-	72	83	67	59
Elongation to Breaking	%	-	150	5	2,5	3
Light Transmission	%	89	91	92	86	89
Refractive Index	%	1,576	1,586	1,489	1,561	1,591

Table 4 shows the five different characteristics in five different polymers.

A lightweight, strong material that stretches rather than breaks, would be ideal. Furthermore, it must have a high light transmission with a low refractive index. Polyethylene Terephthalate (PET) is the heaviest one of the five polymers that are discussed. With the area of the cover measuring 10,3 m², the weight will be a total of 27,6 kg. With its high tensile strength and elongation to breaking, it offers poor light transmission, with a possible 1 000 W/m² coming in, only 890 W/m² will be transmitted once the cover is on – a total loss of 440W loss due to only light transmission. The refractive index is the extent to which light will be bent when passing through the polymer; although it has a low impact, a zero on the refractive index is ideal. Comparing this to polycarbonate (PC), the weight difference at maximum is 2,88 kg, but with its low tensile strength and high elongation to breaking this is more suited for the application. Compared to the light transmission of PET, PC is only two per cent better at 91%. It increases the overall power by 80 W/m² – a loss therefore of only 360W. Poly (methyl methacrylate) (PMMA) is similar in weight to PC, but it has an extremely low elongation to a breaking percentage compared to PC and PET. Although it has a better light refractive index, it is only slightly better than PC. Styrene Acrylonitrile (SAN) resin and general-purpose Polystyrene (PS) are clear polymers that are lightweight, have low tensile strength and an even lower elongation to breaking percentage, combined with a light transmission lower than that of PET.

All things considered, the polymer best suited for the application, will be PC, considerations include that although it is not the lightest and does not boast the lowest refractive index, it has a high elongation to break percentage. Apart from covering the panels, the material must also shield the driver against possible projectiles from oncoming traffic.

4.2 Scale-model setup results

The scale-model instrument was developed to evaluate tracing trough cover material and thus the optimal cover material. It also assists with design for the full-scale bypass diode placements. The scaled instrument evaluations are used to project a possible outcome on full scale.

4.2.1 Custom-scale instrument

As explained in Section 3.2, the custom-scale model instrument was constructed with BPW34 PD sensors used as solar cells, an Arduino to acquire the data, and covered with a curved sheet of polycarbonate.

Figure 40 shows the graphs of the individual rows of PD sensors, the BPW34 as discussed in Section 2.6.2, with the path the light follows through the material.

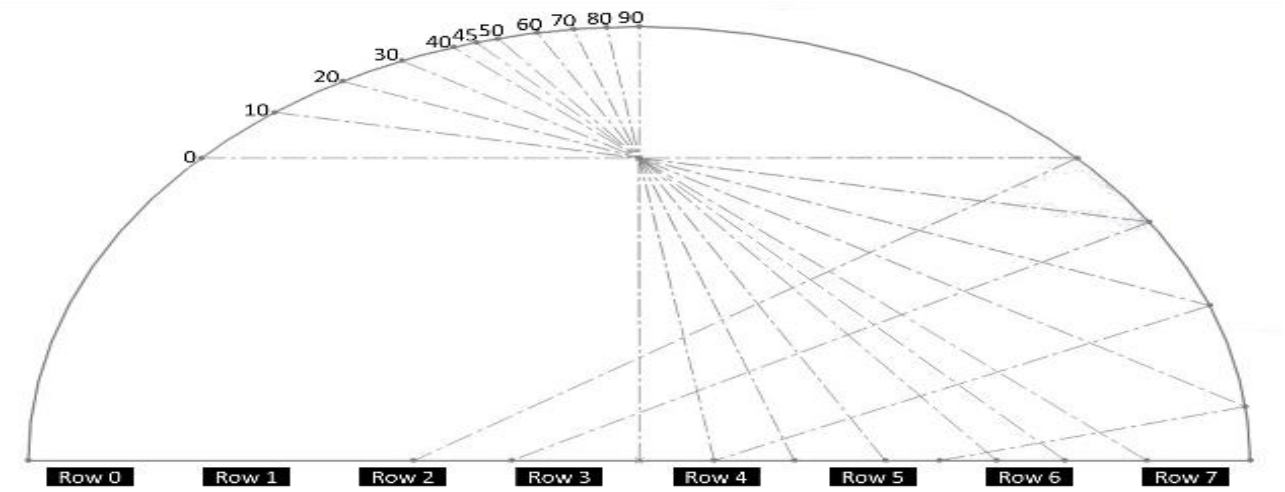

Figure 40 : Ray reflection when light refracts and reflects inside the dome.

Figure 40 depicts the sensor layout from the instruction in Section 3.2.1, and demonstrates an approximate path the light will follow. As seen at the angle 0° – 30°, there is a reflection back to the platform, whereas from 40° –90° the light directly shines on the panels. This angle is in correspondence with the surface of the earth. When for example the sun rises, the angle is at 0°, but by the hour it increases with a few degrees. This setup is to artificially simulate that occurrence. In Figure 40 the sunrise at 0°, then refracts and reflects back to Row 2. For the next 10° it hits between Rows 2 and 3,

at 20° it hits on Row 4, and by 30° it hits close to Row 5. As from 40°, it only refracts and does not reflect from the inside; this means that the light will shine on Row 7, and, as it increases up to 90° the light will hit between Rows 3 and 4.

This experiment involved using the same setup as in Section 3.2.1, but instead of using a bulb, a laser was used to determine the path the light would follow. The laser determined, the path to predict how the light would behave upon entering the vehicle.

4.2.2 Measured irradiance data of the custom-scaled instrument

This section shows and discusses the results of the scaled experiments with the cover on and the cover off.

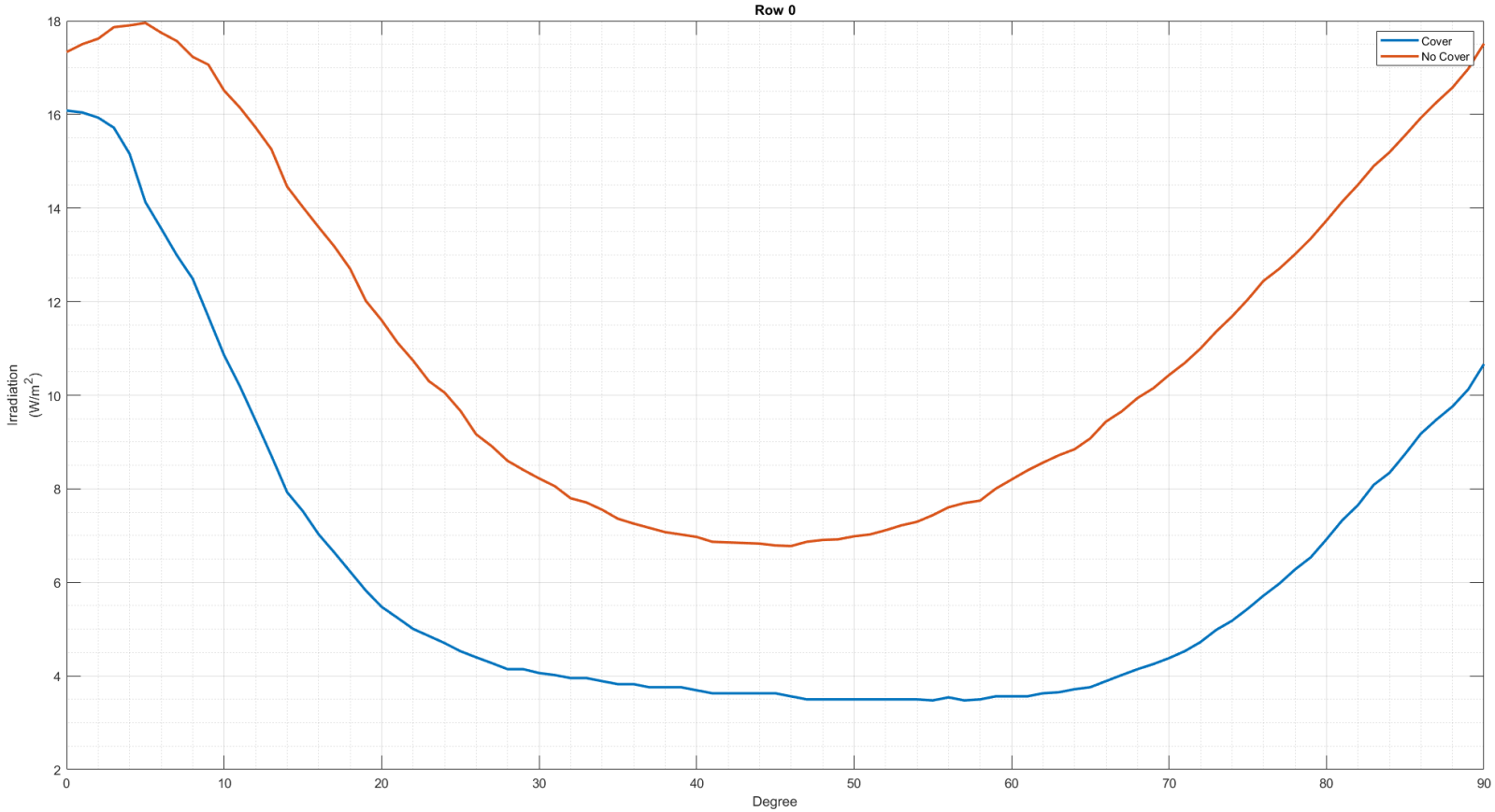

Figure 41 : Row-0 data where the orange line represents the irradiation level with the cover on, and the blue line the irradiation level with the cover off.

Figure 41 displays the data from Row 0, as explained in chapter 3.2. Figure 40 shows that when the light source rises, it starts from the left and rises up and over to the right, corresponding with the numbering from left to right. Row 0 has a maximum irradiation of only 18 W/m². The orange line represents the test performed without the cover, whereas the blue line represents the test performed with the cover on. Between 0° and 8° there is 0,7-W/m² increase in power visible on the orange line, but not on the blue This is due to the beam angle of the bulb, i.e. 35° where sunlight is not be restricted, but on the blue line it must pass through the cover first. This reflects and refracts the light. Between 8° and 45° there is a downward trend as the reflection does not affect the PD as much. Then, again, from 45° up to 90°, there is a steady increase as the actual light starts entering the range of the PD. At 0° 7% more irradiation comes from the 'no cover' reading, and reaches a high of 58% more at the 70° mark.

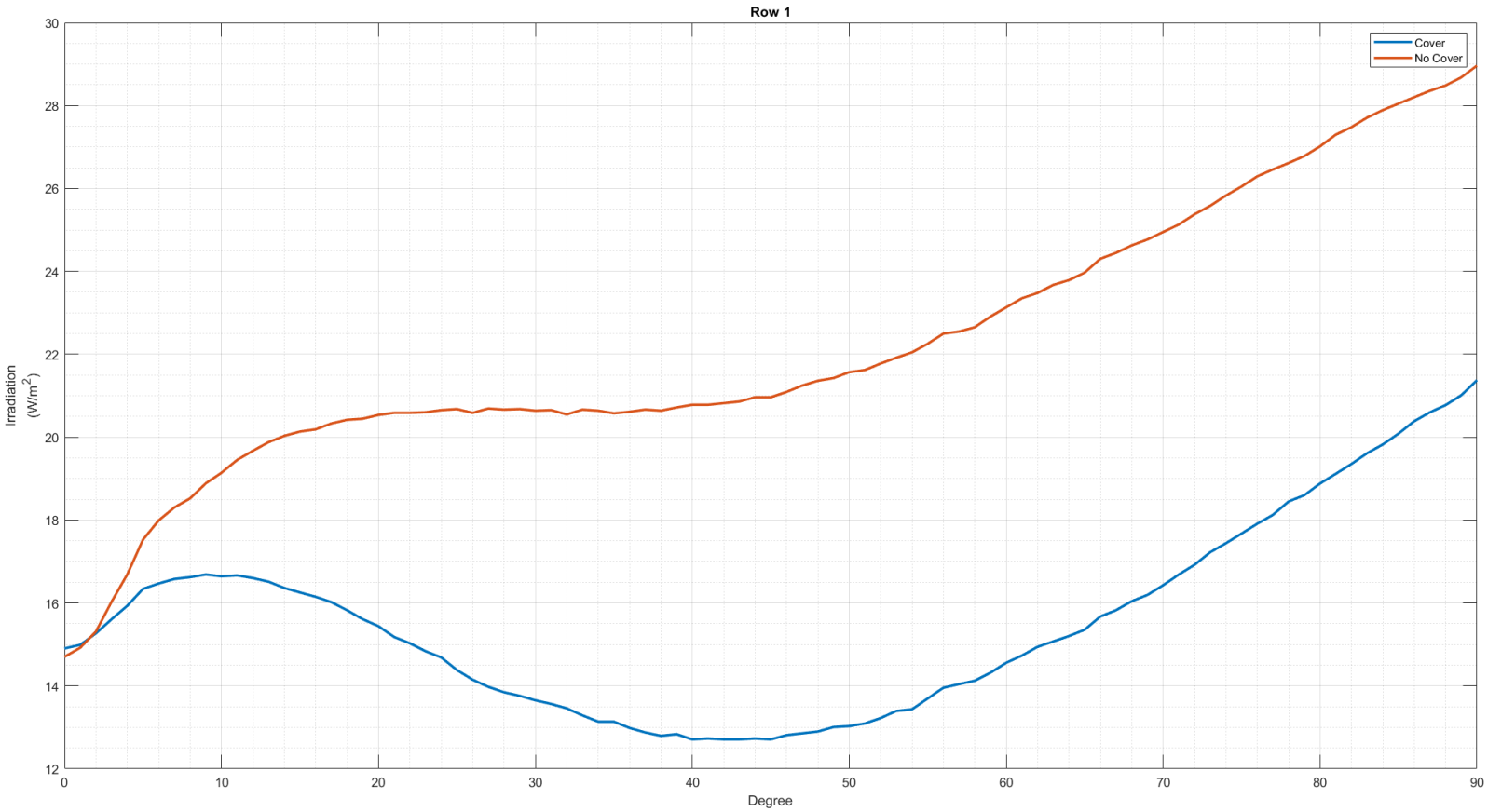

Figure 42 : Row 1 data where the orange line is the irradiation level with the cover on and the blue line is the irradiation level with the cover off.

Figure 42 follows the same pattern as Row 0. The data starts at the approximately same irradiation level as in Figure 41, but it increases and does not drop as dramatically without the cover, compared to when the cover is on. In Figure 40 it is clear that the light moves away from the one side as the irradiation increases, and then back to the middle, causing the dip in Figure 42 with the cover on.

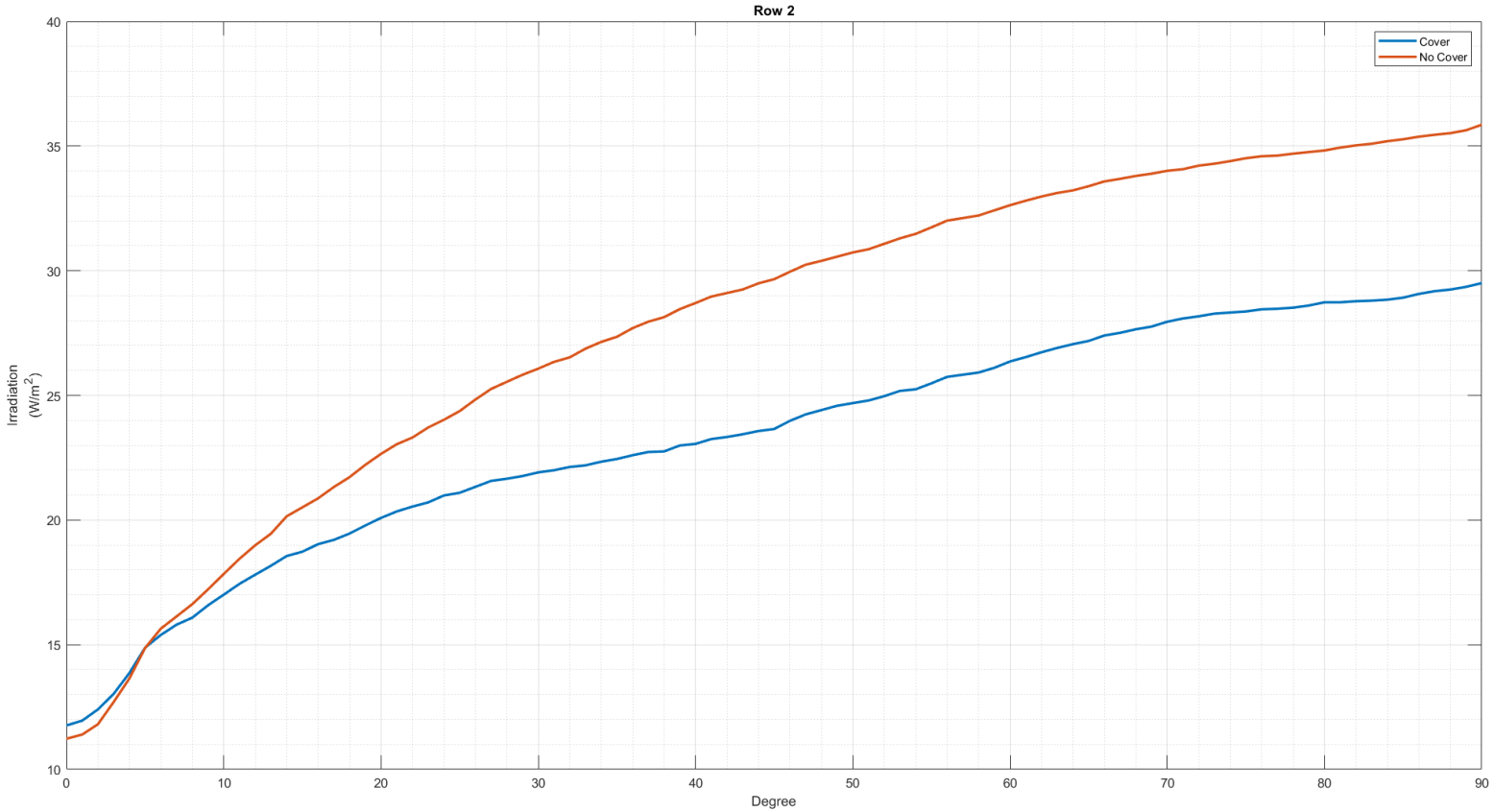

Figure 43 : Row-2 data where the orange line represents the irradiation level with the cover on, and the blue line the irradiation level with the cover off.

Figure 43 shows good correlation up to 10°; thereafter the cover is responsible for a rapid degradation up to 40° where it tents to follow the curve, but at a lower offset. This power loss is because of the physical properties of the cover material

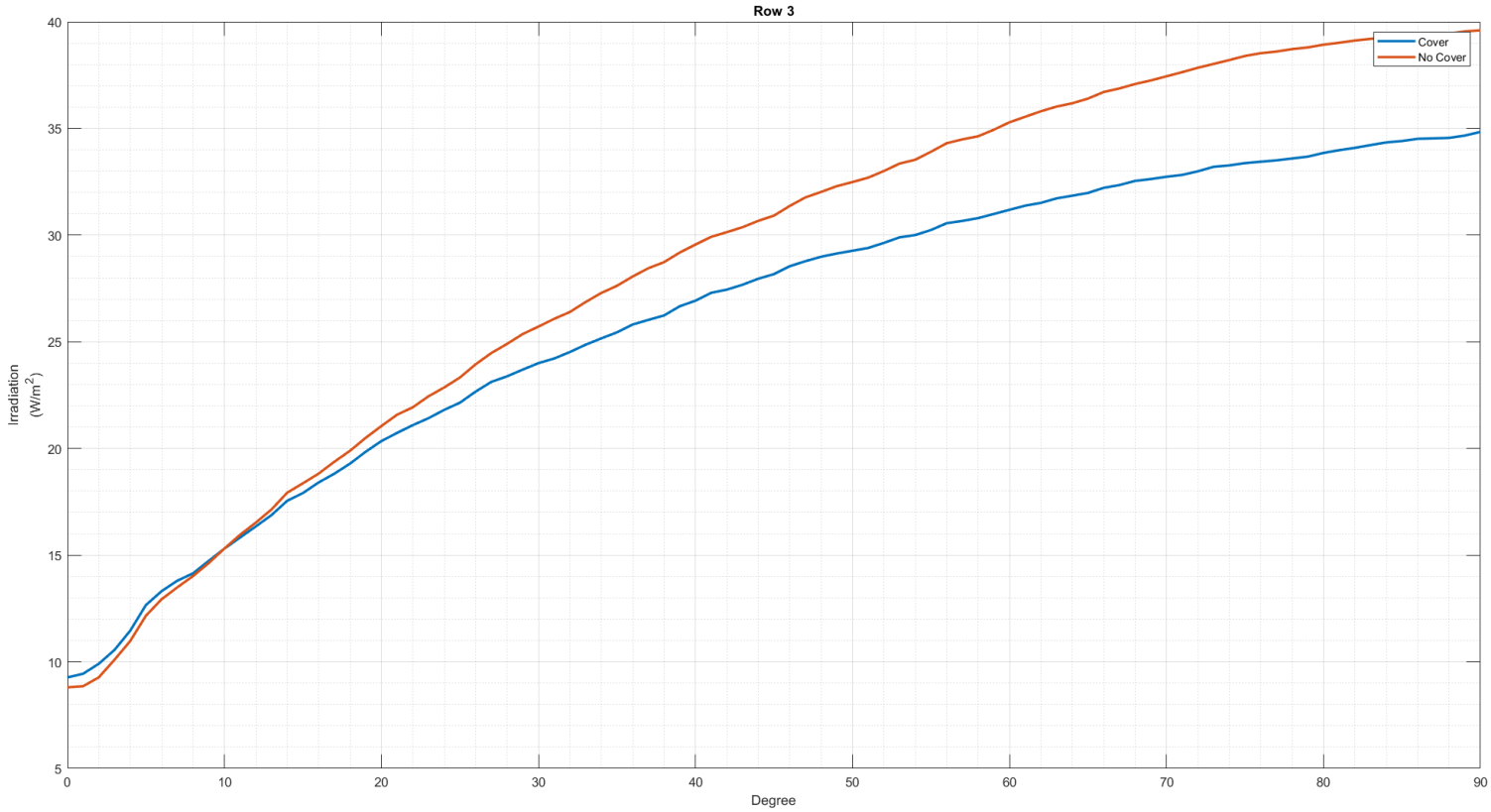

Figure 44 : Row-3 data where the orange line represents the irradiation level with the cover on and the blue line the irradiation level with the cover off.

Figure 44 shows a close correlation up to 10° degrees, from where the irradiation with the cover on, decreases as the angle increases.

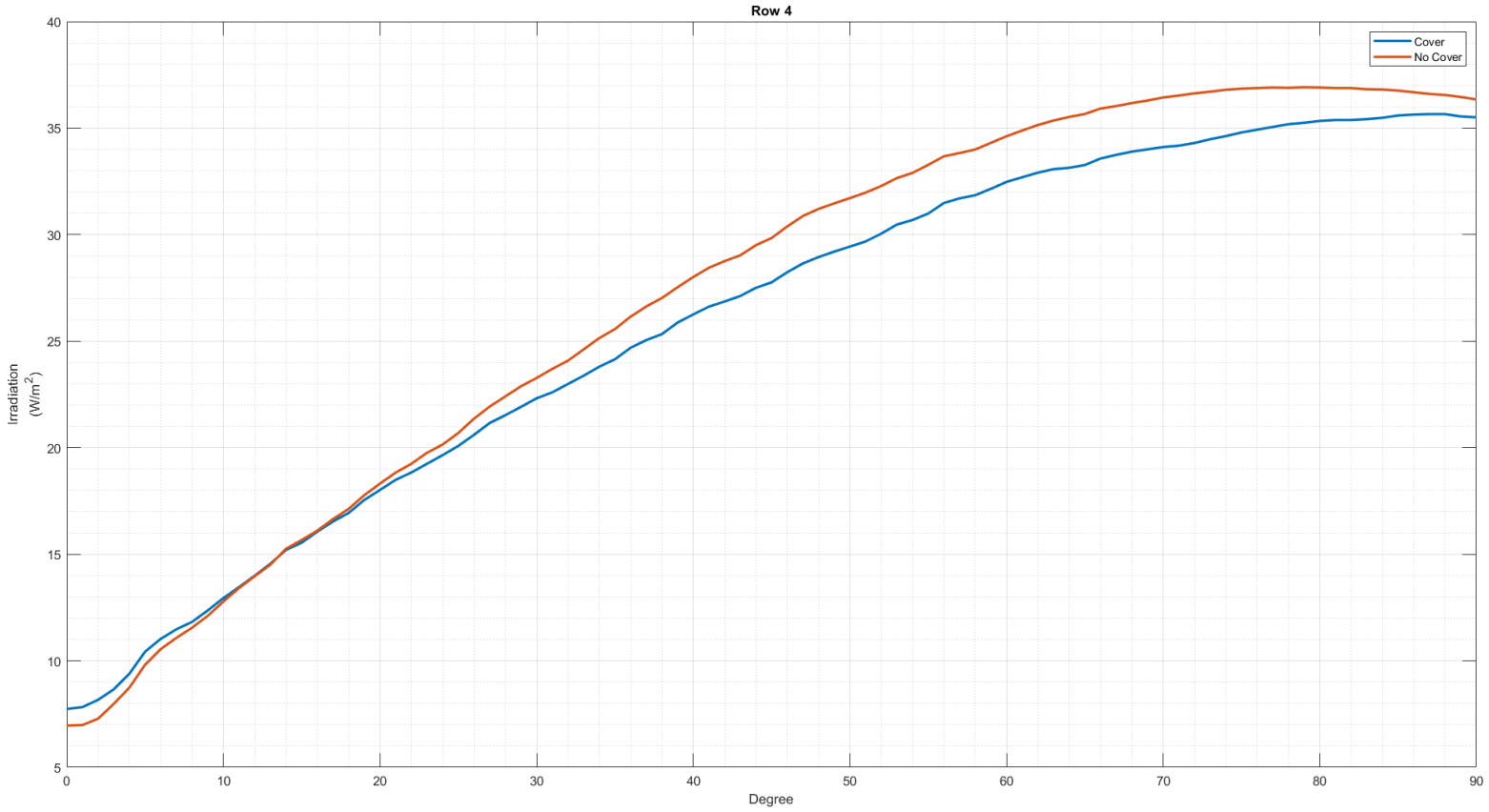

Figure 45 : Row-4 data where the orange line represented the irradiation level with the cover on and the blue line the irradiation level with the cover off.

Figure 45 shows a curve that is expected, where there is a small increase in the irradiation without the cover, compared to with cover. Between 70° and 90° the gap between the two datasets decreased.

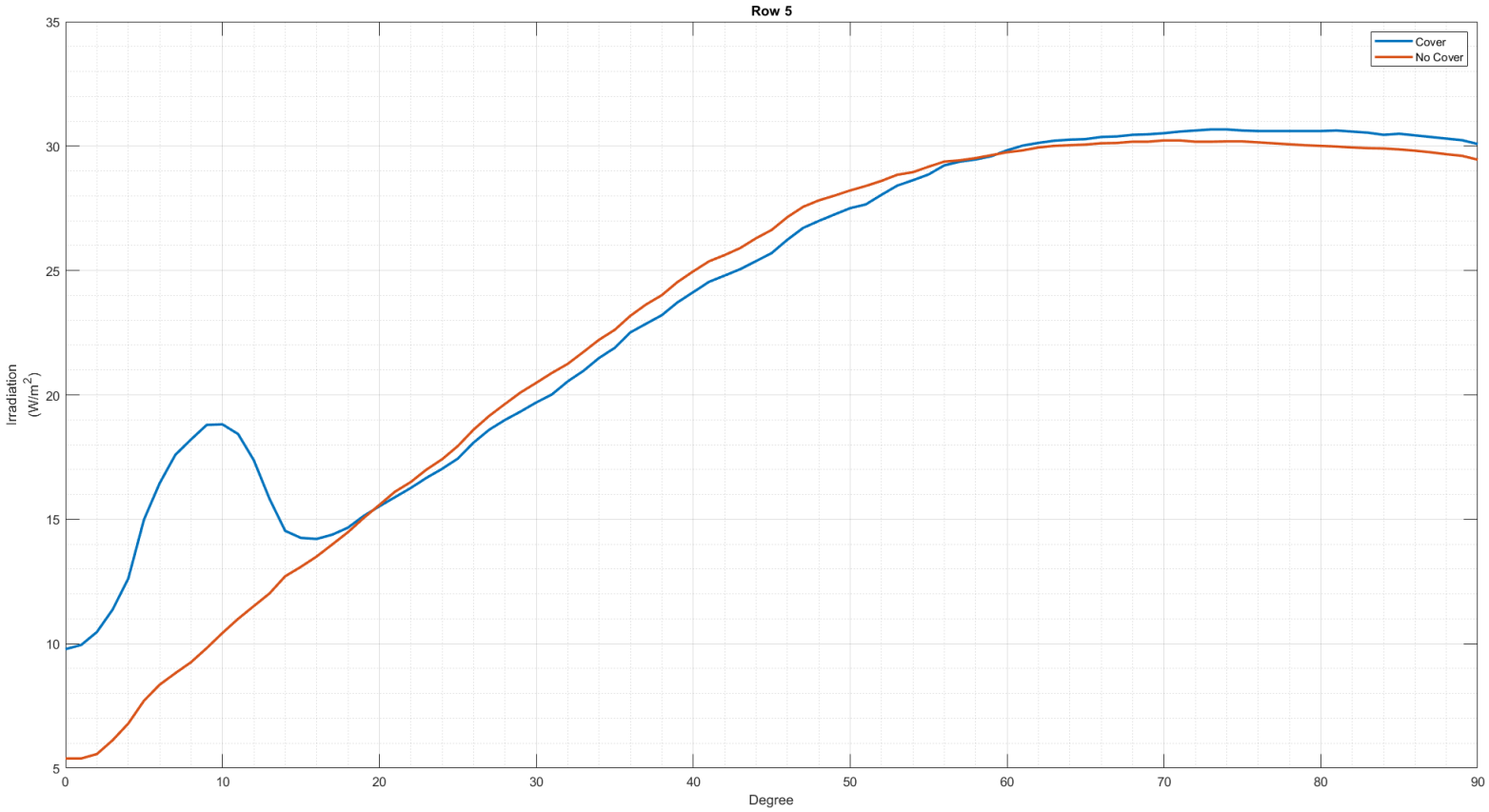

Figure 46 : Row-5 data where the orange line represents the irradiation level with the cover on and the blue line the irradiation level with the cover off.

Figure 46 observes a deviation at 10° where power under the cover is more than that of the power without the cover. This anomaly occurs because of reflection and refraction. As depicted in Figure 40, when the bend in the cover forms a convex lens, the power coming through is more strongly focused on a smaller area; then, as the graph reaches 70°, the cover material once again passes that of the 'no cover', this is again due the focusing.

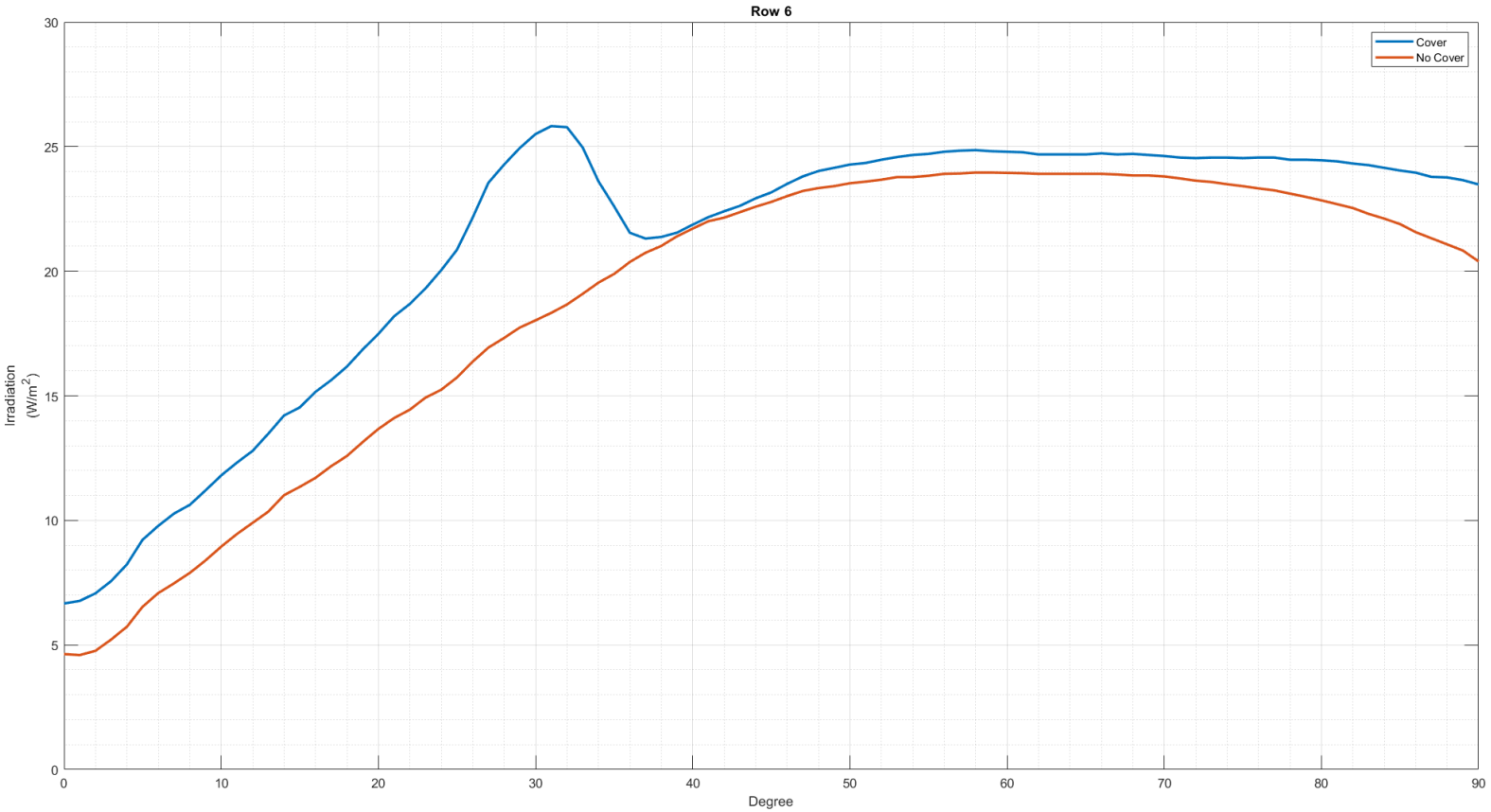

Figure 47 : Row-6 data where the orange line represents the irradiation level with the cover on, and the blue line the irradiation level with the cover off.

In Figure 47 the cover material once again surpasses the no-cover test , with a maximum peak roundabout 30°, but unlike Figure 46 continues to outperform the no-cover test. This is also due to the focusing effect.

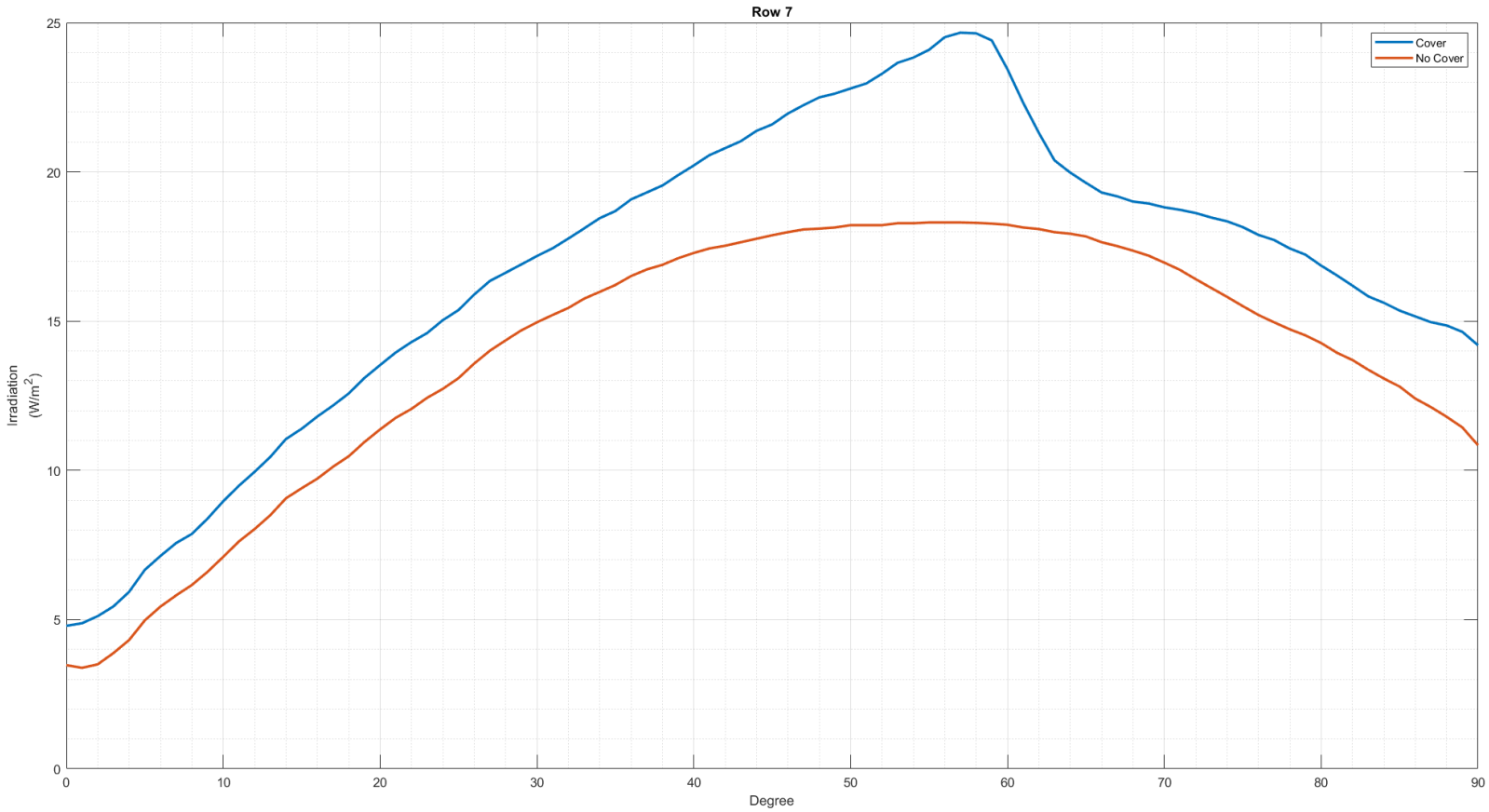

Figure 48 : Row-7 data where the orange line represents the irradiation level with the cover on and the blue line the irradiation level with the cover off.

Figure 48 shows the same effect as in Figure 46, just more prominently. Not only at the graphs, but also the data must be taken into consideration. In Figure 48 the W/m²-peak is 25 W/m², dropping to 19 W/m²; this is why it looks as if the experiment with the cover outperforms the one without the cover. When taking all the data into consideration, there is still a pattern that clearly states that the one with the cover is underperforming by 4%. As explained in the literature, the results from the scale-model instrument should assist in the placement of bypass diodes.

4.2.3 Summary of scale model

The purpose of the scale model is to establish the viability of the theory, as well as to determine the placement of the bypass diodes. It is unknown if the full scale would have the same magnitude of focusing effect. It is significant to show that the focusing effect could generate more power. During the scale-model test the data shows us that there is a small loss – approximately 6% to 10% – over the array of PD. With Rows 1 – 4 having a larger than average loss, Row 5 has very little difference, and in Rows 6 – 8 there is a trend that the power generated under the cover is more than that generated without the cover. This led to the placement of diodes, as Row 1 that had the biggest difference can be bypassed with diodes so as not to pull down the whole array.

4.3 Bypass diodes

As stated in Section 3.3 the bypass diodes are small diodes that look similar to photodiode, but they bypass the cells when there is a shadow over them. These can usually be connected to a series or string of panels, and when a shadow is cast over the panel, they will bypass it so as not to lose the entire string, but only the section connected to the bypass diode. These diodes, however, are expensive. The scale model will indicate where and in which circumstance the bypass diodes are needed. This will then lead to the placement of the diodes as seen in Figure *49*.

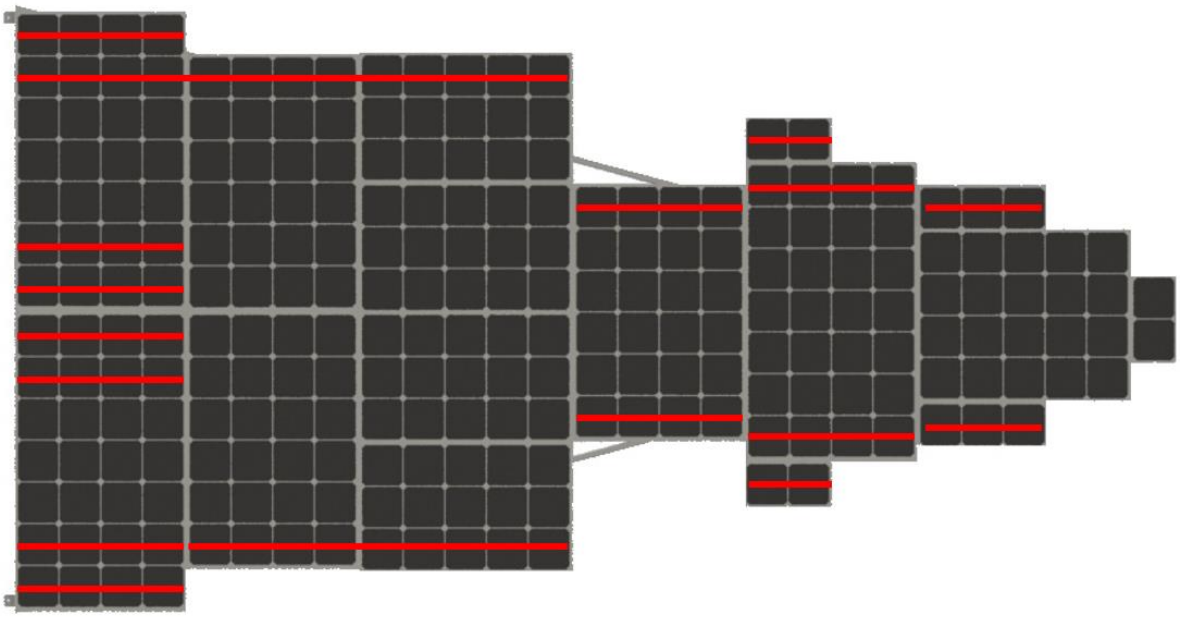

Figure 49 : Layout of the solar array with bypass diodes.

In Figure *49* there are several objects that can cast a shadow on the panels behind. In Figure 49 the proposed layout of the PV Modules. In Figure *49* the red stripes are connected through bypass diodes. The bypass diodes on the side of the array are there to assist in the varied power generation as the sun moves over the array and as the array itself moves.

4.4 Full-scale cover material results

The purpose of this section is to show and discuss the result of the full-scale testing that will also address the uncertainty as depicted in the scale-model results.

The test is performed at the CUT in Bloemfontein, between 07:00 and 17:00. These times were chosen because preliminary experimentation showed that before 07:00 and after 17:00 the MPPT would not be able to detect the trace amounts of power and would shut down.

In this section the efficiency of the vehicle is evaluated, as well as compared to tilt, no tilt, cover and no cover. Then conclusions are drawn, based on the results obtained.

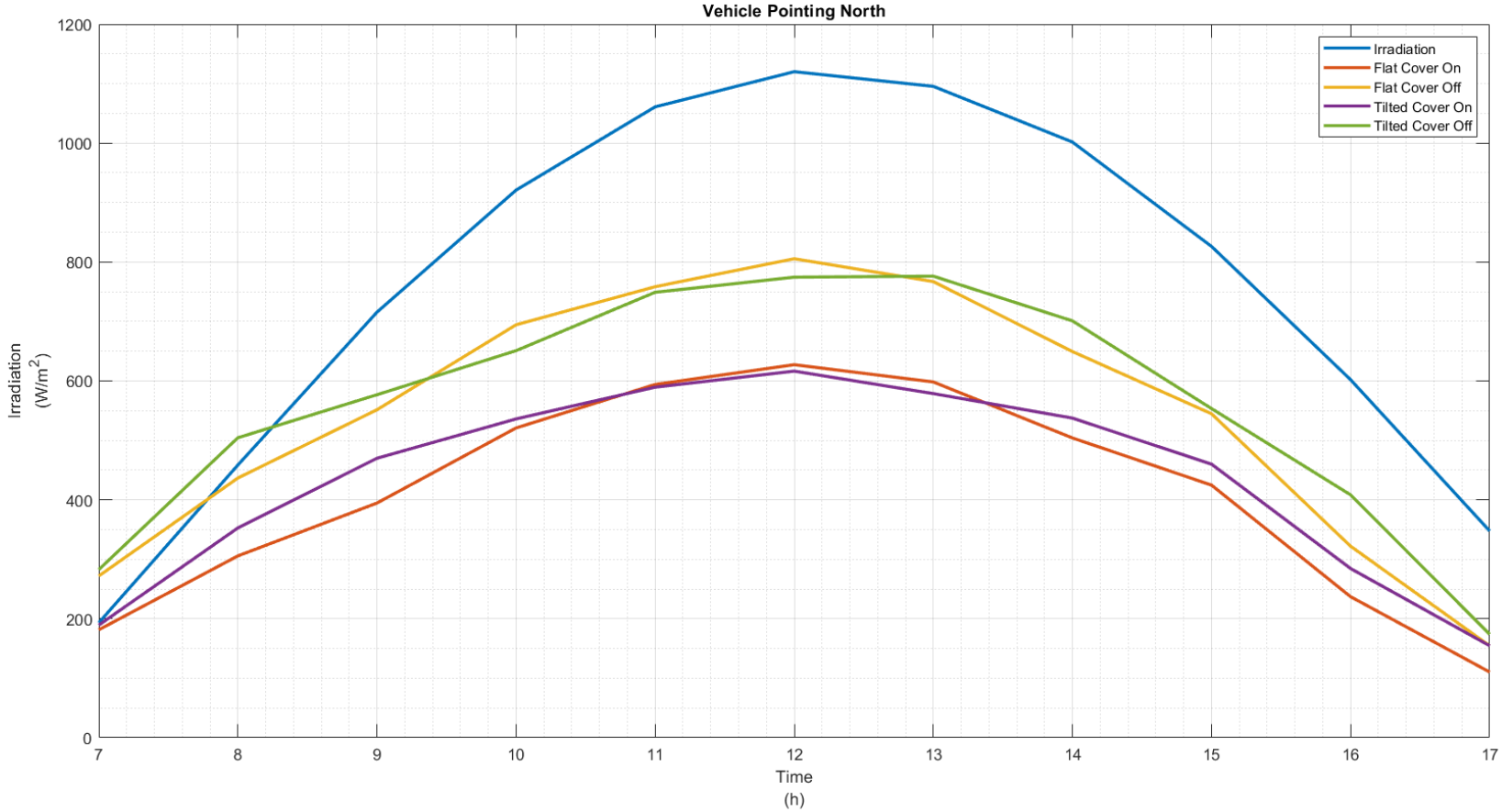

Figure 50 : Vehicle pointing north

In Figure 50 the data is shown for a vehicle sampled with the spreadsheets as shown in Table 3, taking a reading every hour from the MPPT and verifying the data on a fluke 365.

The blue line indicates the irradiation from the sun, this data is obtained from a Campbell Scientific weather station that utilises the CMP100 sensor. At 07:00, the sensor read a radiation of 200 W/m², by noon the irradiations increased to a high of 1 100 W/m², and by late afternoon at the end of the test it reverted to a low of 350 W/m².

As stated in Chapter 3, the vehicle comprises 4m² of solar panels. This equates to a possible maximum of 980W that can be generated. The orange line indicates generation with the cover closed and panels flat, in accordance with the ground level. The power started at just under 200W generated at 07:00, but rose to a mere 627W – only 64% of the 1 000 W/m² these panels are able to generate, bearing in mind that the irradiation is above normal at 1 100 W/m². The yellow line indicates the vehicle with panels flat and no cover on the back. As stated in Chapter 2, there is a 4% loss due to reflection and, and, due to the optical transmittance as explained in Chapter 3, there are also losses not present in this test. Another factor contributing to an increase of up to 805W, is the extreme heat caused by little wind circulation under the cover compared to 'no cover'. The purple line is the one representing the covered vehicle tilted towards the east and later the afternoon towards the west. Up to 11:00 there is a clear increase when the flat solar panel is more effective, as titling it will direct it away from the sun. Just after 13:00, the tilted panel is again more effective. The green line represents the tilted panels under the cover. Similar to the yellow line, the green line performs better than those that are not covered. There is, however, a similar performance that occurs between the flat and tilted panels when the tilted one's dip below the flat ones, but they regain their momentum in the afternoon and generate more power than the flat panels.

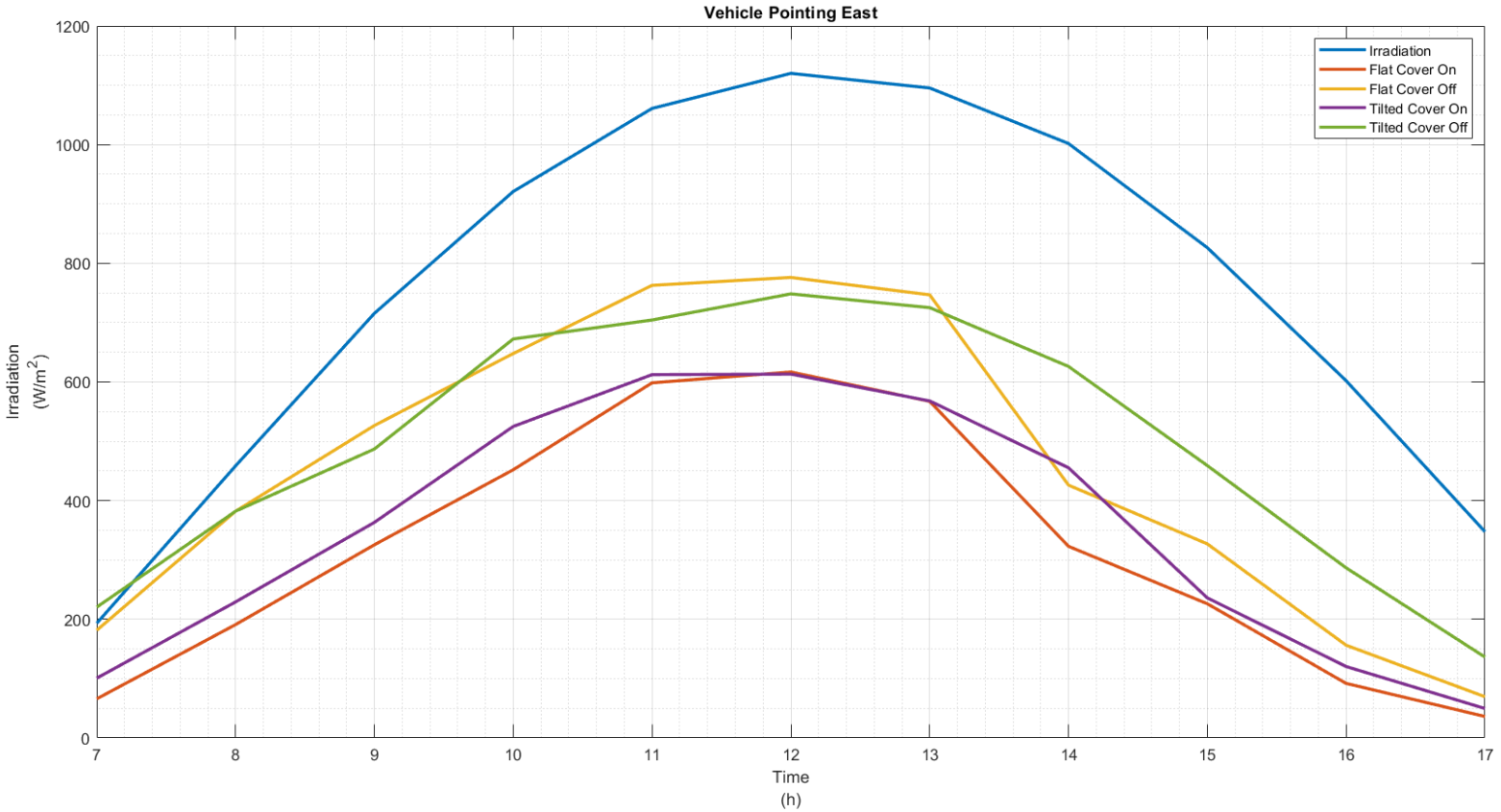

Figure 51 : Vehicle pointing east

Up to 13:00 Figure 51 and 50 show a similar pattern. From 13:00 onwards in the test that the module was flat, there was close to a 50% decrease in power between 13:00 and 14:00 after which the power went on a down curve to lower than that of the tilted panels.

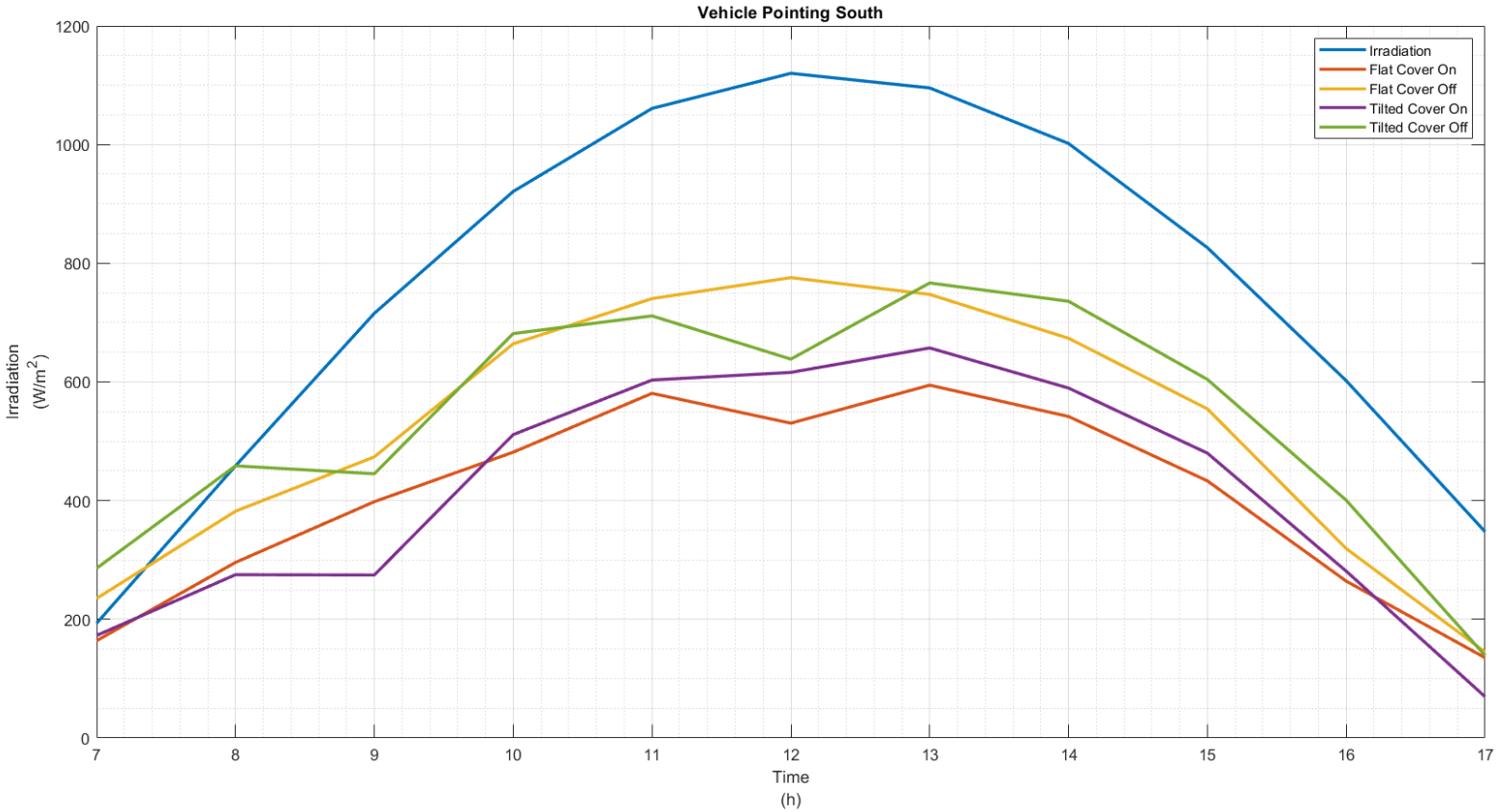

Figure 52 : Vehicle pointing south

In Figure 52 the tilted panel without a cover outperformed the rest. At 09:00 both tilted and with and without a cover showed a dip in power compared to the irradiation slope. This was due to one of the sides casting a shadow on the panels further than that of the bypass diodes.

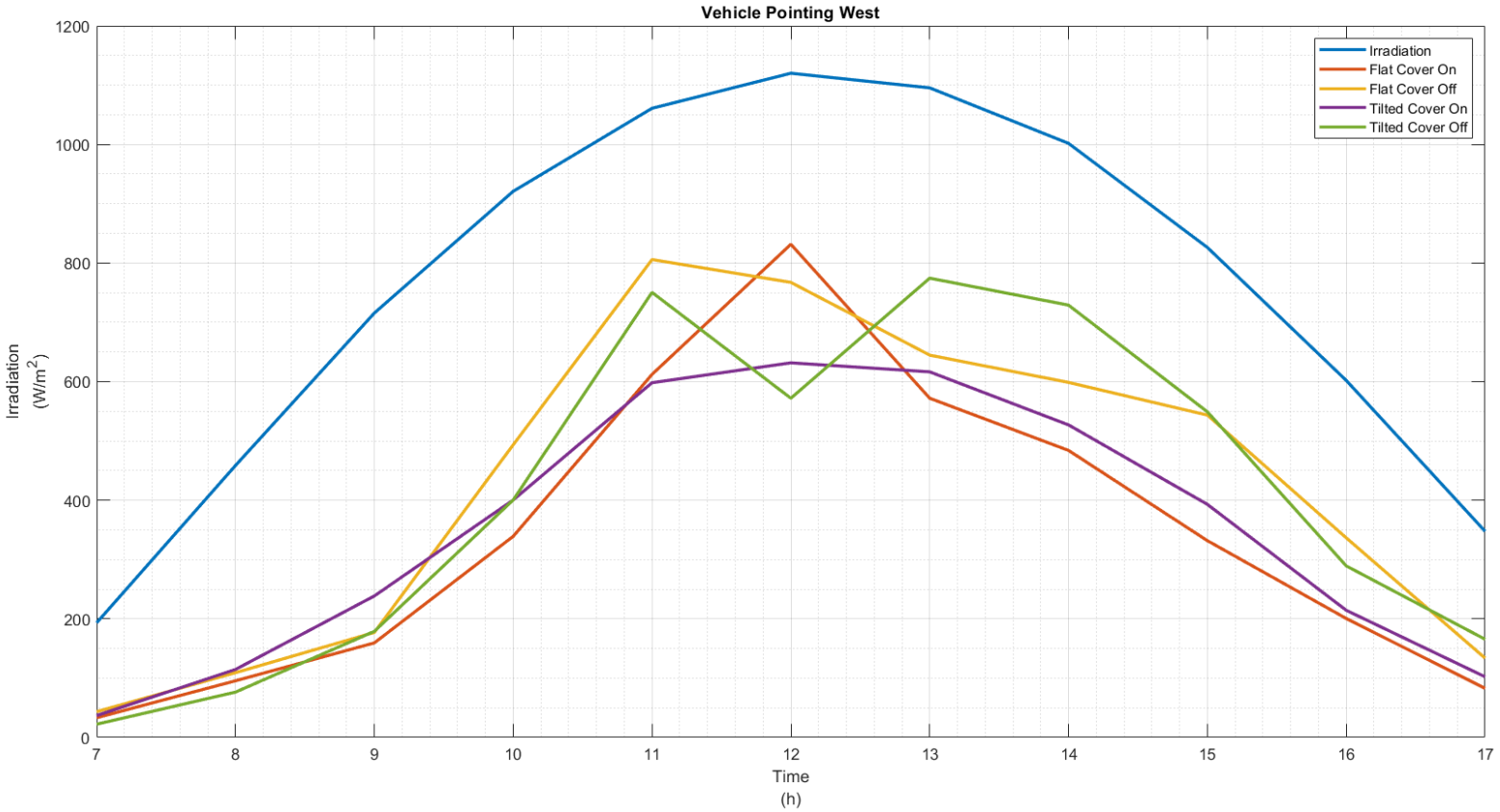

Figure 53 : Vehicle pointing west

Figure 53 demonstrates when the vehicle is casting a shadow on the panels. This is the reason why the day has a slow start compared to other directions. With the sun always at an angle, the irradiation levels seem sporadic between 11:00 and 13:00; this is due to the latitude and longitude of the test. As from 13:00 onwards, the data stabilises and again the 'no cover' has a better energy generating capabilities.

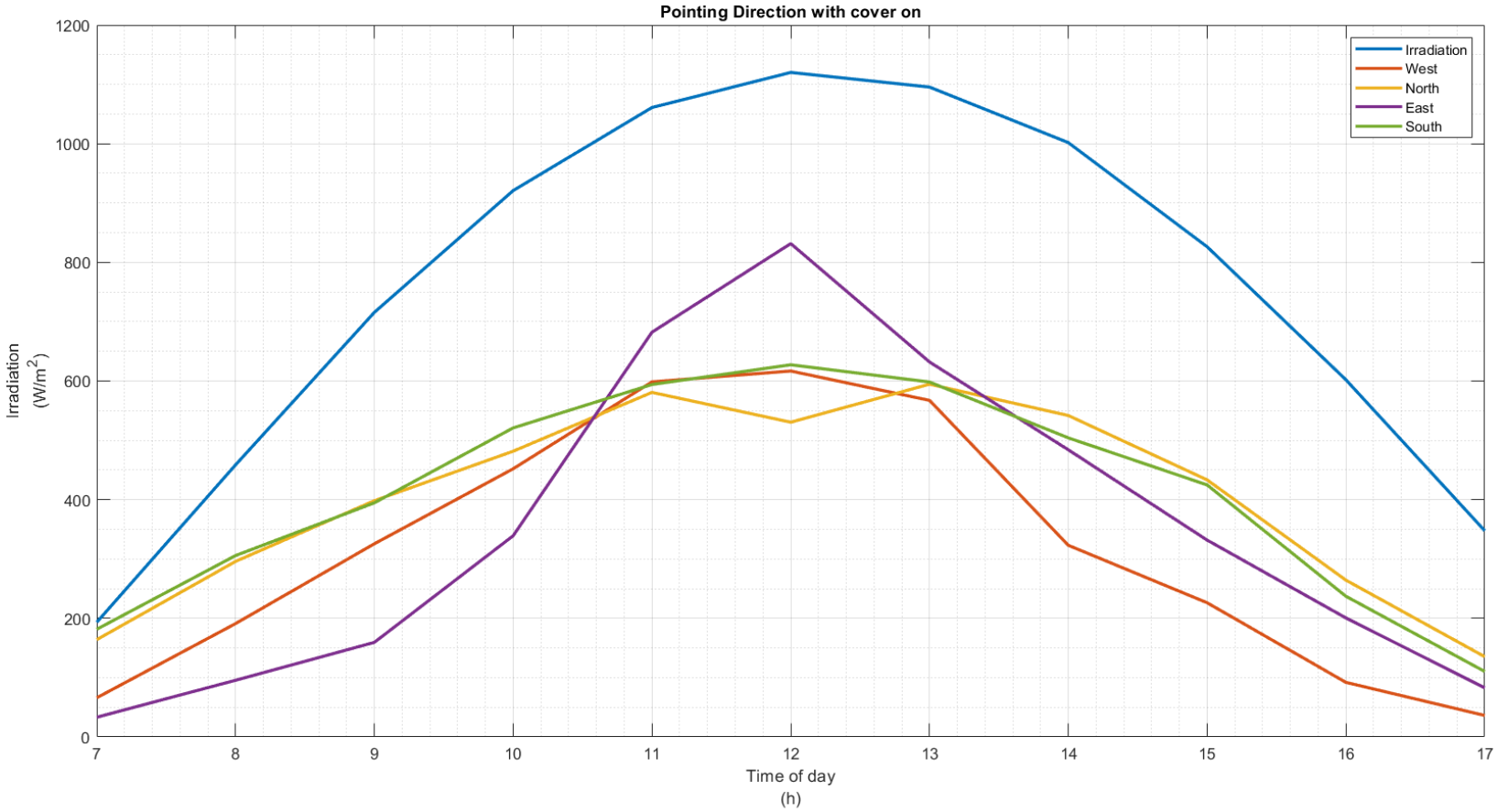

Figure 54 : Vehicle pointing with the cover on

Figure 54 displays the data of the irradiation compared to that with the panels flat in the four desired directions. The blue line in Figure 54 signifies the irradiation from the sun, measured on a CMP100 sensor and then collected by a Campbell Scientific logger. The orange line represents the vehicle pointing west. As the sun rises, it is to the back of the vehicle and will set over the front, possibly casting a shadow of the seat on the panels. The yellow line represents the vehicle pointing north. The sun will rise to the right-hand side of the vehicle and set to the left. The purple line is pointing east; the sun will therefore rise over the front of the vehicle and cast a shadow over the panels in the morning, while it will be concentrated in the afternoon. The green line denotes the vehicle pointing south, with the sun rising to the left and setting to the right.

The green and yellow lines both have the sun from the side for the entire day. However, as the testing area is at 23° latitude, and corresponds with the elevation angle (as seen in Section 2.5.3), it means that at 12:00 the sun is not perpendicular to the earth but a few degrees to the north. This is evident in the data collected between 07:00 and 11:00. The data mostly correspond – the small variations are due to the curvature of the dome. At 12:00 there is a drop in power on the yellow line, but an increase in the green. This is because of the sun that is more to the north, casting a small but notable shadow over the panels. The orange line has a steady incline, but less than that of the yellow and green lines. This is due to the thickness of the plastic at the angle of inclination, since the dome slopes at a lower angle to the rear than it does to the side. In the afternoon again, the shadow is cast onto the seat and the power generated, is influenced. The purple line demonstrates the same effect only in reverse, as the vehicle is pointing towards the sun. At first the seat side performs poorly, but sharply increases performance when the sun is high enough to pass over the seat. Contributing to this increase in performance, is the fact that here the plastic at inclination angle is very low. The internal reflection also helps to create a high-performance point in the vehicle.

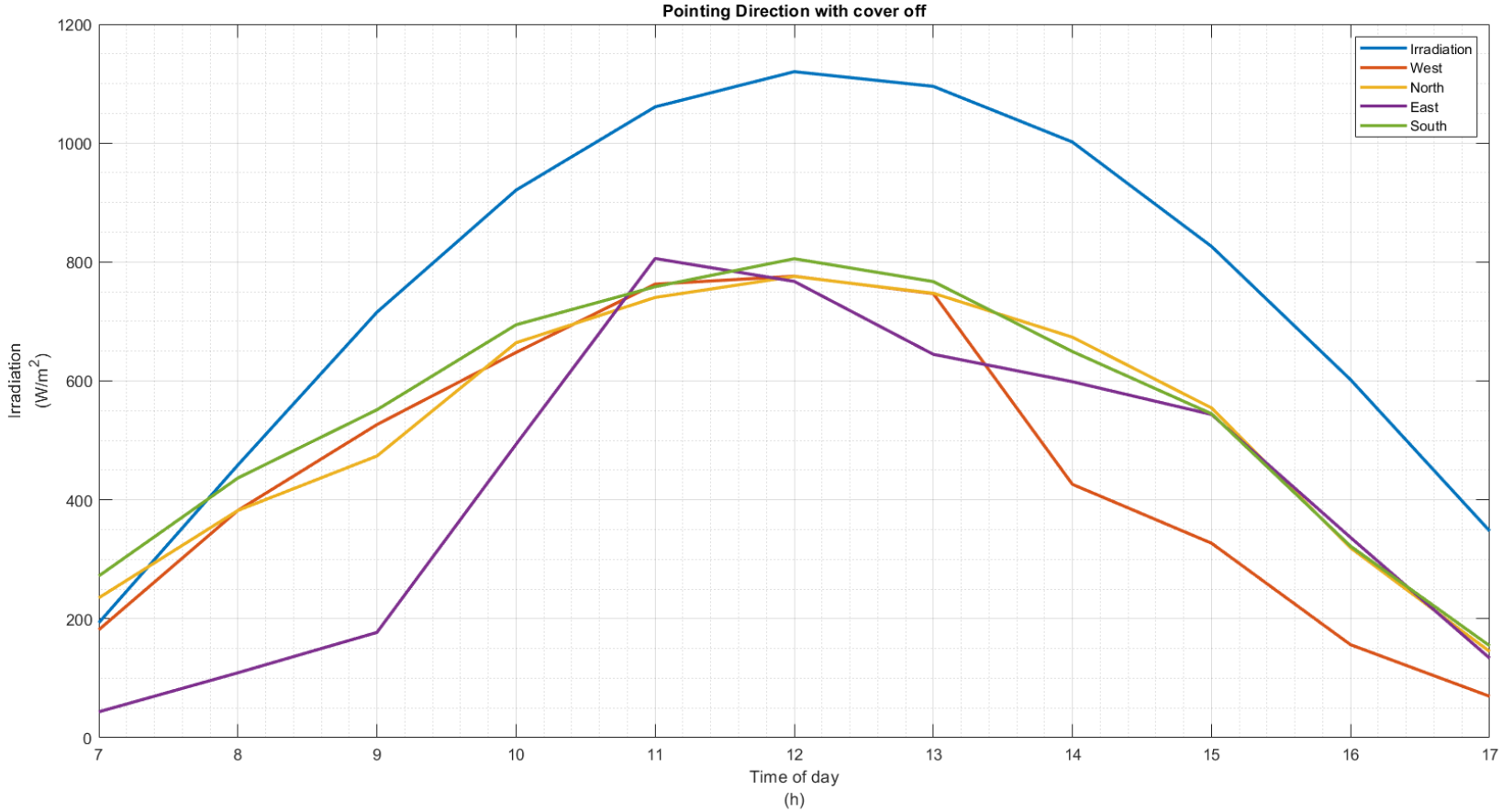

Figure 55 : Vehicle pointing with the cover off

Figure 55 displays the power generated in each orientation with the cover off, whereas Figure 54 displays the orientation with the cover on. The general graph is similar to that of Figure 54 with only a few minor differences that will be discussed later.

As indicated by the legend in the top right-hand corner, the blue line indicates the irradiation measured by a CMP100 sensor and logged onto a cable scientific logger. This data is important for the comparison to the operation of the PV module. Normal PV modules power rating is measured when the irradiation is 1000 W/m². Whereas here the power generated is measured when the irradiation is 240 W/m².

The orange line reflects that the orientation of the vehicle is west and that a shadow will be cast over the seat when the sun starts setting. This is evident in the orange graph from 13:00 to 17:00, where the line is below the rest of the lines. The inverse is true for the purple line representing the eastern orientation. The purple line is well below the rest in the morning, since the sun rises over the cab and casts a shadow over the PV modules. The yellow and green lines respectively represent the northern and southern orientation. Both indicate that a steady day, with a normal trend. There is a small decrease in the slope on the yellow line at 09:00, but it soon recovers due to high clouds noted at the time.

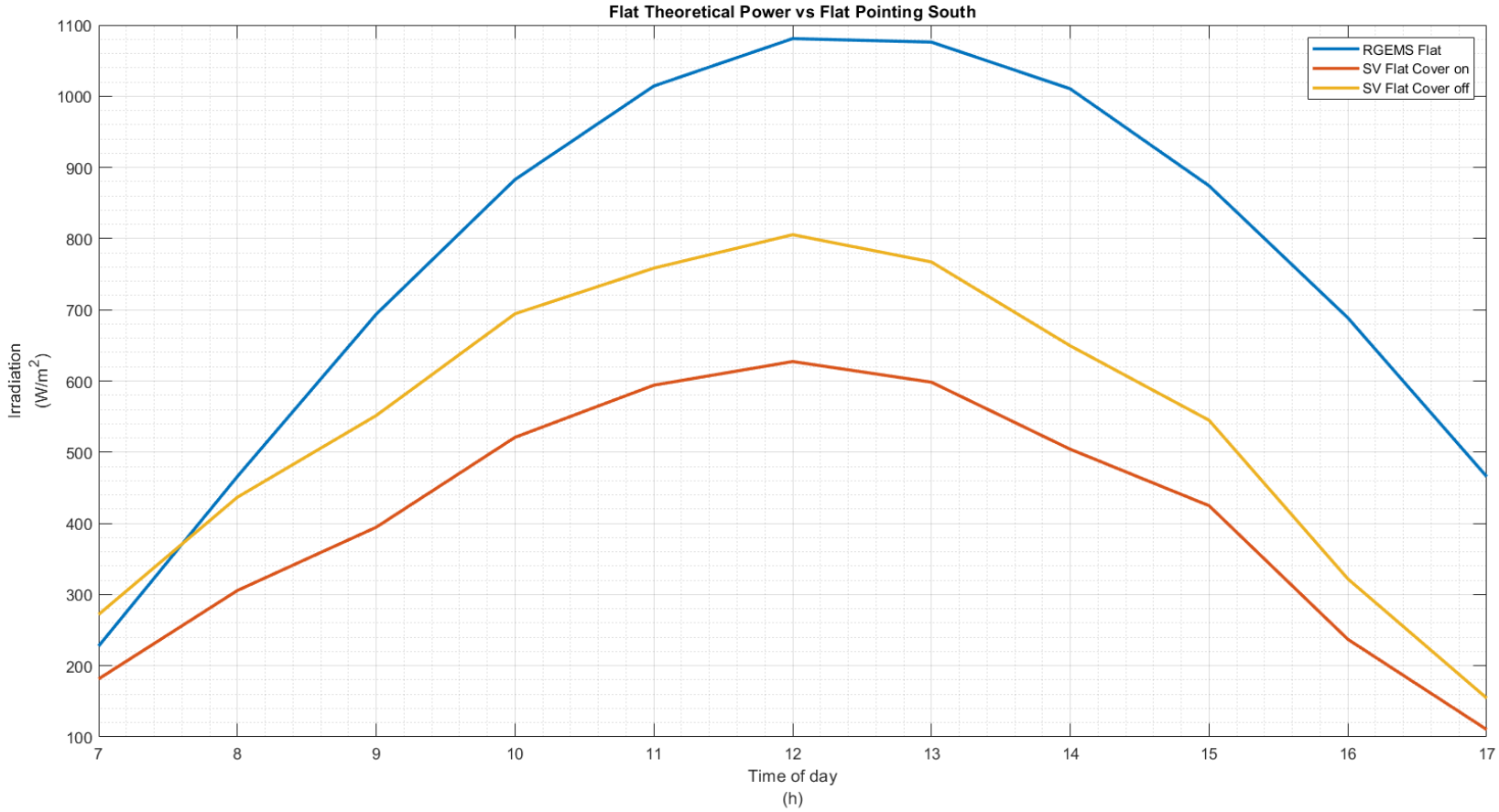

Figure 56 : Theoretical power vs power actually generated

The blue line represents the maximum capacity of power generated without any losses. It combines irradiation and the maximum power the solar panel is capable generating.

4.5 Comparison between the scaled instrument and full-size solar challenger vehicle

The purpose of this section is to show and discuss the difference or correlation in data gathered from the scale instrument compared to data gathered form the full-scale vehicle.

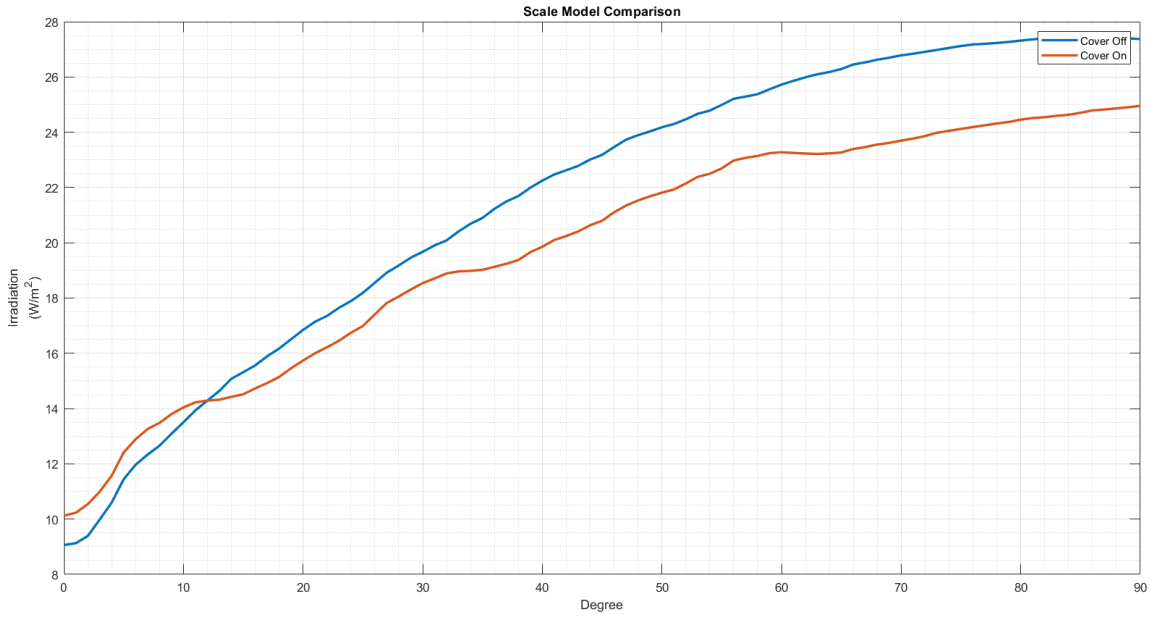

Figure 57 : Test graph of test Instrument

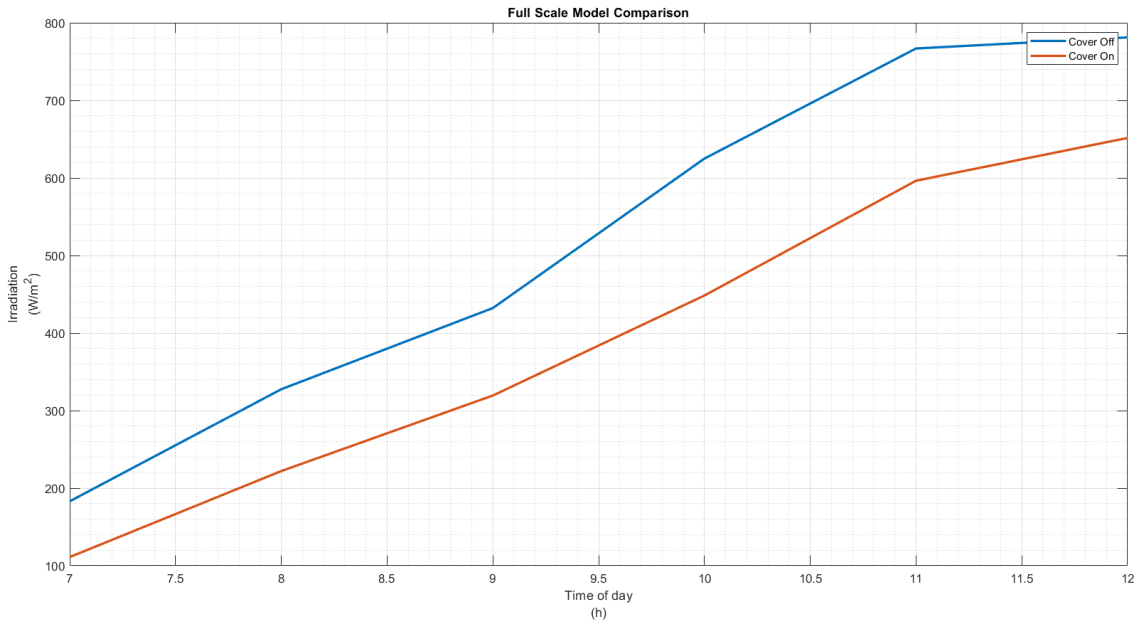

Figure 58 : Test graph of vehicle

Figure 57 shows the difference between having the cover on and having the cover off. According to Figure 57 there is an average difference of just below 10%, compared to the cover graph.

Figure 58 shows the graph of the test vehicle data collected. Measured over panels in flat orientation, there is a 26,5% difference with the cover on compared to the cover off.

Table 5 : Scale model compared to full-scale model.

		Scale Model			Full-scale Model		
Time	Degree	Cover	No cover	% Increase	Cover	No cover	% Increase
7h00	21°	16,0 W/m²	17,1 W/m²	6,7%	181,5 W/m²	272,0 W/m²	33,3%
8h00	35°	19,0 W/m²	20,9 W/m²	9,0%	305,7 W/m²	436,8 W/m²	30,0%
9h00	48°	21,5 W/m²	23,9 W/m²	9,9%	394,6 W/m²	551,5 W/m²	28,4%
10h00	62°	23,2 W/m²	26,0 W/m²	10,6%	520,9 W/m²	694,4 W/m²	25,0%
11h00	75°	24,1 W/m²	27,1 W/m²	11,1%	594,1 W/m²	758,5 W/m²	21,7%
12h00	84°	24,6 W/m²	27,4 W/m²	10,2%	627,3 W/m²	805,5 W/m²	22,1%
13h00	75°	24,1 W/m²	27,1 W/m²	11,1%	598,3 W/m²	767,1 W/m²	22,0%
14h00	62°	23,2 W/m²	26,0 W/m²	10,6%	504,1 W/m²	649,4 W/m²	22,4%
15h00	49°	21,7 W/m²	24,0 W/m²	9,8%	424,8 W/m²	544,8 W/m²	22,0%
16h00	35°	19,0 W/m²	20,9 W/m²	9,0%	237,1 W/m²	322,0 W/m²	26,4%
17h00	22°	16,2 W/m²	17,4 W/m²	6,5%	110,4 W/m²	154,5 W/m²	28,6%

By taking the calculations in Section 2.5 into consideration, the first column (time of day) can be converted to a degree of incidence (Column 2). In doing so, a direct correlation can be drawn between the scale model and full-scale model.

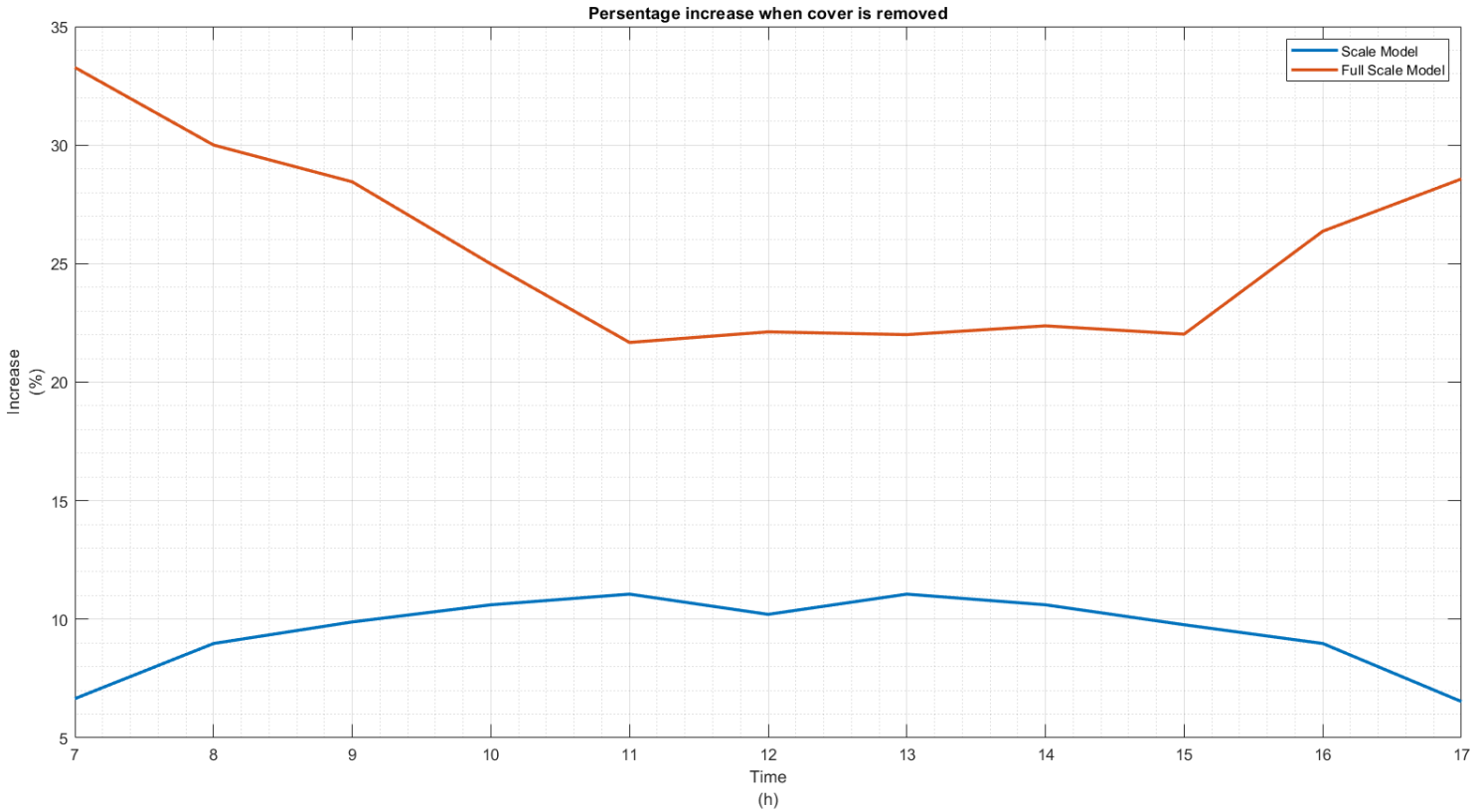

Figure 59 : Power output with cover on compared to that of 'no cover'

Figure 59 is a graph indicating the increase in power when the cover is removed, for both scale model as well as the full-scale model.

The scale model is represented in the blue line, which starts low and shows a slight increase to just above 11%. Then it drops to almost 10% and again increases to 11% only to drop down to 6%.

The full-scale model behaves in an opposite manner. It starts at 33%, drops to 22% then again increases to 28%.

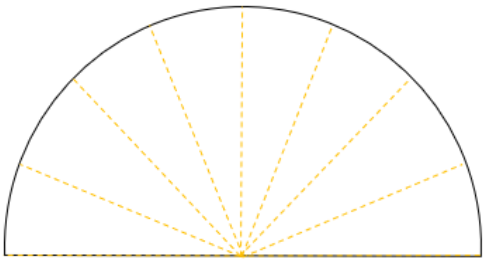

Figure 60: Scale model dome

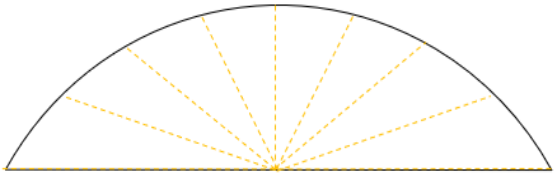

Figure 61: Scale-model dome

Figure 60 depicts a round dome, similar to the dome on the scale model. The flatter dome in Figure 61 is the one on the full-scale model. The round cover has stronger internal reflection than the flat one. As the full-scale model is the actual vehicle that was used in the Sasol Solar Challenge, the cover is scratched, causing lower transparency and more refraction. The solar vehicle is equipped with bypass diodes, and the cover is held in place by ribs. One of the ribs can cover a bypass diode and will also cause a dip in generated power.

4.6 Concluding remarks

In this chapter the results are discussed on solar tracking, which include solar tracking with and without a cover. It starts with the methods of reviewing the comparison of the cover material with the ideal choice – being polycarbonate – with elongation to breaking and high light transmission. This assists of solar tracking with the cover. The scale model setup results showed how the light will behave when inside the canopy, and these results consequently led to the ideal placement of the bypass diodes. It was observed on-scale that internal reflection outperformed the positive 'not covered' results at specific angles. Results have shown a noticeable loss under the cover due to refraction and outer reflection of light from the polycarbonate. In addition, the heat generated inside the vehicle that cannot escape from under the cover, hampers airflow inside and over the panels.

Chapter 5: Conclusion

The purpose of this dissertation is to evaluate and compare solar tracking towards a competitive solar challenger race vehicle. The results generated and discussed, led to designing considerations and improvements. Evaluation includes solar tracking under a transparent aerodynamic dome that reduces the driving force to reduce the drag, but at the possible cost of generation losses of the material used. The study led to developing evaluation and comparison methods, as well as to discussions on the corresponding results, of the advantages of solar tracking which include an aerodynamic dome tracking application. In order to evaluate solar tracking and solar tracking under a dome application, one firstly needs to identify an optimal transparent cover material for the dome; this is followed by test methods, as well as the design and construction of test instrumentation that would lead to results generation. Results show and discuss scaled and full-scale testing, including evaluation of the gains and losses of solar tracking with and without the aerodynamic dome. It is unclear how the shape of the dome affects the individual cells of the photovoltaic module; on full scale setup sense experimentation was done on a full-power generation connection. One should note that the small-scale experimentation showed an unexpected increase in power generation with the cover on, but only at certain reflection angles and that this was not observed on full scale. Reasons for this increase could include the shape of the dome on scale, which had a sharper curve angle. One could consider this for future dome designs on the full-scale model, which could lead to the same power gains seen on the small scale. This study contributed with methods to evaluate and compare solar tracking power generation, with and without coverings, and material suggestions for a competitive solar vehicle or similar domed application. The test instrument designed, is significant in that it provides different test method options to evaluate solar tracking and cover material selection or tracing tests. Considering all the data gathered and reviewed, solar tracking is proven as an optimal power generation solution but, the advantages gained from tracking under a cover were not enough to justify drag coefficient gains at low speeds and windless days. This, however,

needs to be reconsidered in new aerodynamic designs or for high-speed applications. One should also consider that, with solar vehicles becoming mainstream in future, the need to be able to evaluate solar tracking solutions would become more imperative.

Future studies could include, but is not limited to, the influence of the cooling effects of airflow on panels with tracking hampered by covers, comparisons of drag versus generation in high-speed vehicle application or in windy conditions, and possibly the consideration of aerodynamic stability versus power generation. Similarly ¼ wavelength anti- reflecting coating for the cover material, and using high-emissivity polymers to reduce the temperature in the dome. Future study can include on table 5 to add the irradiation level measured from the pyranometer, thus the reflection can be accurately determined.

Chapter 6: References

[1] SASC, “Sasol solar 2018", 2018. [Online]. https://www.solarchallenge.org.za/solar-challenge/regulations [Accessed: 7 May 2022]

[2] N.A. Kelly and T.L. Gibson, “Improved photovoltaic energy output for cloudy conditions with a solar tracking system". *Sol. Energy*, vol. 83, no. 11, pp. 2092 – 2102, 2009.

[3] L.P. Lewis Fraas, "*Solar Cells and Their Applications.",pp. 67-110,* 2010.

[4] H.E. Fabrication, “The Importance of Surface Recombination and Energy-Bandgap Narrowing in p-n-Junction Silicon Solar Cells", *IEEE Trans. Electron Devices*, vol. ED-26, no. 9, pp. 1294 – 1298, 1979.

[5] R. Santbergen and R.J.C. van Zolingen, “The absorption factor of crystalline silicon PV cells: A numerical and experimental study", *Sol. Energy Mater. Sol. Cells*, vol. 92, no. 4, pp. 432 – 444, 2008.

[6] The Editors of Encyclopaedia Britannica, “Polycarbonate,” *Encyclopedia Britannica*, 2017. [Online]. Available: https://www.britannica.com/science/polycarbonate. [Accessed: 11Mar 2020].

[7] S.-J. Park and M.-K. Seo, *Interface Science and Technology,vol.18, pp. 431-499*. 2011.

[8] J. McMurry, *Organic Chemistry*, 7th ed., pp.1242-1256. 2008.

[9] D.W.W. van Krevelen, *Properties of Polymers*. pp. 49-66. 1997.

[10] G.-S. Plastic Optics, “Transmission Curves”. [Online]. Available: https://www.gsoptics.com/transmission-curves. [Accessed: 7 May 2022]

[11] J.D. Muzzy, *Comprehensive Composite Materials, vol 2, pp. 57-76*. 2000.

[12] The Editors of Encyclopaedia Britannica, “Polymethyl Methacrylate,” *Britannica*. 2018. [Online]. https://www.britannica.com/science/polymethyl-methacrylate. [Accessed: 7 May 2022]

[13] R.T. Morrison and R.N. Boyd, *Organic Chemistry*, 6th ed. Asoke K Ghosh, 2002.

[14] G. R. Mitchell, “Structure of Polymer Glasses: Short-range Order", in *Encyclopedia of Materials: Science and Technology*, Elsevier, 2001, pp. 8926–8932.

[15] The Editors of Encyclopaedia Britannica, “Polyethylene Terephthalate,” *Britannica*. 2018. [Online]. https://www.britannica.com/science/polyethylene-terephthalate [Accessed: 7 May 2022]

[16] Nudec, “Product range PETg SANuv.” [Online]. https://www.nudec-plastic.com/products/plastic-sheets-san-acrylonitrile-styrene [Accessed: 7 May 2022]

[17] J.M. Margolis, “Polyethylene Terephthalate", *Eng Thermoplast*. pp. 1 – 17, 1985.

[18] The Editors of Encyclopaedia Britannica, “Styrene-acrylonitrile copolymer", *Britannica*. 2018. [Online]. https://www.britannica.com/science/styrene-acrylonitrile-copolymer [Accessed: 7 May 2022]

[19] B.P. Federation, “Styrene Acrylonitrile (SAN)", 2019. . [Online]. https://www.bpf.co.uk/plastipedia/polymers/SAN.aspx [Accessed: 7 May 2022]

[20] J.A. Brydson, “Plastics Based on Styrene", in *Plastics Materials*, Elsevier, 1999, pp. 425 – 465.

[21] The Editors of Encyclopaedia Britannica, “Polystyrene,” *Britannica*. 2018. [Online]. https://www.britannica.com/science/polystyrene [Accessed: 7 May 2022]

[22] L.W. McKeen, “Plastics Used in Medical Devices", *Handb. Polym. Appl. Med. Med. Devices*, pp. 21 – 53, 2014.

[23] S.-K. Lin, *Handbook of Polymers*. George Wypych, ChemTec Publishing, 2012.

[24] Polymerdatabase, “POLYMERIZATION OF STYRENE", *Polymer Properties Database*, 215AD. .

[25] M. Burghoorn, *et al.*, “Single layer broadband anti-reflective coatings for plastic substrates produced by full wafer and roll-to-roll step-and-flash nano-imprint lithography", *Materials (Basel).*, vol. 6, no. 9, pp. 3710–3726, 2013.

[26] C.G. Parazzoli, R.B. Greegor, K.Li, B.E.C. Koltenbah, and M.Tanielian, “Experimental Verification and Simulation of Negative Index of Refraction Using Snell’s Law", *Phys.*

Rev. Lett., vol. 90, no. 10, p. 4, 2003.

[27] I. Sarbu and C. Sebarchievici, “Chapter 2 - Solar Radiation", in *Solar Heating and Cooling Systems*, I. Sarbu and C. Sebarchievici, eds. Academic Press, 2017, pp. 13 – 28.

[28] C. Honsberg, “Properties of Sunlight", 2015. .

[29] B. Alsadik, “Chapter 4 - Observation Models and Least Squares Adjustment", in *Adjustment Models in 3D Geomatics and Computational Geophysics*, vol. 4, B. Alsadik, ed. Elsevier, 2019, pp. 89–151.

[30] J.G. Cerón-Bretón, R.M. Cerón-Bretón, M. Rangel-Marrón, M. Muriel-García, Cordova-Quiroz A.V., and A. Estrella-Cahuich, “International Journal of Energy and Environment", vol. 5, no. 3, pp. 328 – 336, 2011.

[31] S.C. Bhatia, “2 - Solar radiations", in *Advanced Renewable Energy Systems*, S. C. Bhatia, ed. Woodhead Publishing India, 2014, pp. 32 – 67.

[32] V. Cvjetkovic, “Overview of architectures with Arduino boards as building blocks for data acquisition and control systems", *2016 13th Int. Conf. Remote Eng. Virtual Instrum.*, no. February, pp. 56 – 63, 2016.

[33] Arduino, “Arduino - Home", *Hardware*. p. 1, 2016. [Online]. https://www.arduino.cc/en/hardware. [Accessed: 7 May 2022]

[34] H. Bayhan, “Forward and reverse current – voltage – temperature characteristics of a typical BPW34 photodiode", vol. 50, pp. 1563 – 1566, 2006.

[35] S.C. Solanki, S. Dubey, and A. Tiwari, “Indoor simulation and testing of photovoltaic thermal (PV / T) air collectors", *Appl. Energy*, vol. 86, no. 11, pp. 2421 – 2428, 2009.

[36] C.D. Elvidge, D.M. Keith, B.T. Tuttle, and K.E. Baugh, “Spectral identification of lighting type and character", *Sensors*, vol. 10, no. 4, pp. 3961 – 3988, 2010.

[37] Y. Tanaka and K. Matsuo, “Non-Thermal Effects of Near-Infrared Irradiation on Melanoma", *Break. Melanoma Res.*, no. June, 2011.

[38] A. Patil, K. Haria, and P. Pashte, “Photodiode based pyranometer". pp. 29 – 33, 2013.

[39] Kipp & Zonen, “Pyranometers For the Accurate Measurement of Solar Irradiance", pp. 1 – 5, 2015.